MODELING PERFORMANCE IMPROVEMENT OF HIGH SPEED BOATS RUNNING ON AN OUTBOARD ENGINE

EUGENE GATETE

MASTER OF SCIENCE
(Mechanical Engineering)

JOMO KENYATTA UNIVERSITY OF AGRICULTURE AND TECHNOLOGY

2019

Modeling Performance Improvement of High Speed Boats Running on an Outboard Engine

Eugene Gatete

A thesis submitted in partial fulfillment for the degree of Master of Science in Mechanical Engineering in the Jomo Kenyatta University of Agriculture and Technology

2019

DECLARATION

This thesis is my original work and has not been presented for a degree in any other university.

Signature..... Date.....

Eugene Gatete

This thesis has been submitted for examination with our approval as the University Supervisors:

Signature..... Date.....

Eng. Dr. Hiram M. Ndiritu

JKUAT, Kenya

Signature..... Date.....

Dr. Robert Kiplimo

JKUAT, Kenya

DEDICATION

This work is dedicated to my lovely and precious wife , Mrs. Antoinette Karemera, my daughter Ange Gladys Gatete Kundwa, Hon. Innocent Kayitare family and my family members for being there for me all through my studies.

ACKNOWLEDGEMENTS

My greatest gratitude goes to the Almighty God and my Savior Jesus Christ for His divine protection and guidance throughout my study. I'm grateful to my supervisors, Eng. Dr. Hiram M. Ndiritu and Dr. Robert Kiplimo for their supervision and assistance throughout my study period. I as well thank Dr. Onesmus M. Muvengei for his continual guidance and encouragement during my study. I thank the University of Rwanda (UR), and the Mobility to Enhance Training of Engineering Graduates in Africa (METEGA) for supporting me financially during my study. I also appreciate Mr. Gerald J Odhiambo, Mr. Enock Obwogi and Mr. Evans Kibiru for their special assistance during my research period. My final thanks goes to all my co-Mechanical Engineering postgraduate students, and all my well-wishers.

TABLE OF CONTENTS

LIST OF TABLES

LIST OF FIGURES

LIST OF APPENDICES

LIST OF ABBREVIATIONS

ANSYS	Finite Element Analysis Software
CAD	Computer Aided Design
CCM	Computational Continuum Mechanics
CFD	Computational Fluid Dynamics
DES	Detached Eddy Simulations
DNS	Direct Numerical Simulations
HSC	High Speed Craft
IGES	Initial Graphics Exchange Specification
JKUAT	Jomo Kenyatta University of Agriculture and Technology
LES	Large Eddy Simulation techniques
METEGA	Mobility to Enhance Training of Engineering Graduates in Africa
RANS	Reynolds Averaged Navier Stokes
RPM	Revolutions per Minute
SIMPLE	Semi-Implicit Method for Pressure-Linked Equations algorithm

LIST OF SYMBOLS

D	Overall diameter of propeller [m]
δ_{ij}	Kroneker delta and is equal to unity when $i = j$, and zero when $i \neq j$
F_i	the external body forces in the i^{th} direction and
g	Acceleration due to gravity [m/s^2]
g_i	the gravitational acceleration in i^{th} direction
η_o	Open Propeller Efficiency [%],
J	Advance coefficient [constant]
Kq	Torque coefficient [%]
Kt	Thrust coefficient [%]
μ	Viscosity of water [m$^2/s$]
N	Rotational speed of the propeller [rev/sec]
p	static pressure [Pa]
P	Total static pressure [Pa]
Po	Absolute pressure at shaft centre [Pa]
Pv	Vapour pressure at ambient temperature [Pa]
Q	Propeller shaft torque [Nm]
ρ	Mass density of water [kg/m^3]
$\bar{\rho}$	time averaged value of density component
σ	Cavitation number [constant]
t	time variable [second]
T	Propeller axial thrust force [N]
$\bar{u}$	time averaged value of velocity component in x-axis
$\bar{u'}$	time averaged value of the fluctuating velocity in x-axis
V	Boat Speed [Knot],
$\bar{v}$	time averaged value of velocity component in y-axis
$\bar{v'}$	time averaged value of the fluctuation velocity in y-axis
x	x-axis coordinate
y	y-axis coordinate

ABSTRACT

The marine propeller is among the most important components of the outboard engine. It transmits power by converting rotational motion into thrust. Blade cavitation in high-speed boats has been found to reduce the performance of the propeller since it results in blade erosion and corrosion, induced vibration and noise. This leads to an inefficient propeller for an outboard engine which in turn causes fuel wastage, high power consumption, harmful emissions and boat accidents. Research have shown that the affected propeller reduced the performance of the outboard propulsion system in transmitting power to move a boat forward. There is therefore a need to improve the efficiency of the propeller for an outboard engine. The improved outboard marine propeller is one way which can be adapted for use in high-speed boats running on an outboard engine. In this research, an outboard marine propeller model was designed, modeled and its performance analyzed, with the focus of improving the performance of the propeller for a high speed boat running on an outboard engine. This is expected to result to reduced fuel consumption due to improved efficiency. A geometric model of the outboard propeller with three blades was modeled in SolidWorks 2017 software. Number of the blades and pitch-to-diameter ratio was designed, modeled and the open water propeller performance assessment of each parameter has been tested. The flow around rotating outboard propeller model was analyzed as the advance coefficient increased in the steady state using RANS equations solved through simulation. The effect of rotational speed on open water propeller performance was also evaluated. The open water propeller performance was evaluated in terms of marine propeller performance characteristics (thrust coefficient (K_T), torque coefficient (K_Q), and open water efficiency (η_0)) as the advance coefficient (J) increased in the commercial software STAR-CCM+ version 9.06. The computation results indicated that the region of recirculation varied on both sides of the blades based on variation in advance coefficient. An evaluation of the propeller performance was carried out by studying the effect of blade number. 3, 4 and 5 blades were tested. The numerical results showed that a decrease in a number of the blades causes an increase in efficiency of more than 6%. This was found for the propeller with three blades which had the best open water propeller performance characteristics. The numerical simulation performed to study the pitch-to-diameter ratio (P/D) on the propeller performance proved that an increased pitch-to-diameter ratio caused an increase in efficiency of approximately 15%. Moreover, the numerical results showed that an increase in rotational speed cause a negative effect on propeller performance. This was observed in the decreased performance characteristics (K_Q and K_T) of open water propeller as the rotational speed increased. The propeller performance characteristics of the improved outboard propeller were compared with historical experimental results of a conventional marine propeller. It is projected that the results of this study will help marine engine manufacturers to design efficient marine propellers. Consequently, this will also help the marine engine and high-speed boat industries to reduce maintenance expenses that occur due to frequent replacement of outboard propellers.

CHAPTER ONE
INTRODUCTION

1.1 Background

The outboard engine shown in Figure 1.1 (a) is an internal combustion engine, used as the modern propulsion power source for small vessels such as high-speed boats. It also has a variety of options to select from; direct-injection two-stroke to a four-stroke cycle, outputs from 2 to 557 horsepower (hp) and weights from a few kilograms to half a metric ton (Lewis, Cleve, H.L Nguyen, H.E. Addy, T.H. Bond, C.M. Lee, , & Chun, 1987). There are various types of outboard engines in the market which vary in size, weight, output and design (Department of the Environment and Water, 2007; H. Yanagi, 2018). The outboard engine is widely used as a power source for slow, medium and high-speed boat or ships. This is due to its high performance, lower cost, simple installation, reduced fire risk, lower weight, higher speed, superior maneuverability, less draft giving better shoal water capability, and easier launching and beaching (Rainbow, 1963). Yamaha, Honda, and Suzuki from Japan; and Mercury and Evinrude from America are the leading manufacturers (Sterling, 1920). A marine propeller is generally fitted to the lower part of an outboard engine shown in Figure 1.1 (a) where it operates in water that has been disturbed by the high-speed boat as it moves in open water as shown in Figure 1.1 (b). When a propeller moves rapidly in the water, the blades are affected by cavitation, which results to inefficiencies. Cavitation is a fluid mechanics phenomenon, which occurs whenever there is fluctuation in the pressure field and/or the velocity of the fluid. In some regions, the flow conditions cause the absolute pressures in the fluid to fall below its vapour pressure. This results in the fluid boiling even at ambient temperature therefore undergo cavitation. Cavitation involves small vapour bubbles called “cavities” forming within the fluid (Basumatary Jahnabi, Wood, 2017). The cavitation causes a decrease in propeller performance characteristics, that is, thrust coefficient (K_T), torque coefficient (K_Q) and open water efficiency (η_0) of the outboard engines (Dubbioso, Muscari, & Di Mascio, 2014). This reductions lead to an increase in fuel and power consumption, and harmful emissions (Helal, Ahmed, & Banawan, 2018). The other effects of cavitation includes loss of speed and damage to the propeller blades result in an inefficient propeller (Yu, Zheng, & Yao, 2006).

To reduce these effects, the outboard marine propeller performance requires to be improved, as efficient propulsors for high-speed boats are in great demand. Reynolds-

Averaged Navier-Stokes (RANS) method has become a practically useful tool to get an efficient marine propeller geometry design which replaces the methods based on the potential theory (Hai-Long, Obwogi, & Yu-Min, 2016; Mintu, 2011). Currently, with the accessibility to superior hardware, it is possible to model the complex fluid flow problems like marine propeller flow and open water performance (M.Bhanu Priya , K.Mohan Krishna, 2015; Hally, 2013; Wang & Walters, 2012; Bartee & J., 1997). The performance improvement of the outboard propeller is the key focus in this study. However, for simplicity of the structural analysis, parameters such as centrifugal stress stiffening, coriolis force, gyroscopic force, temperature and blade twist/ untwist were not considered in this work mainly because they have minor effect on propeller performance characteristics (M.Bhanu Priya , K.Mohan Krishna, 2015).

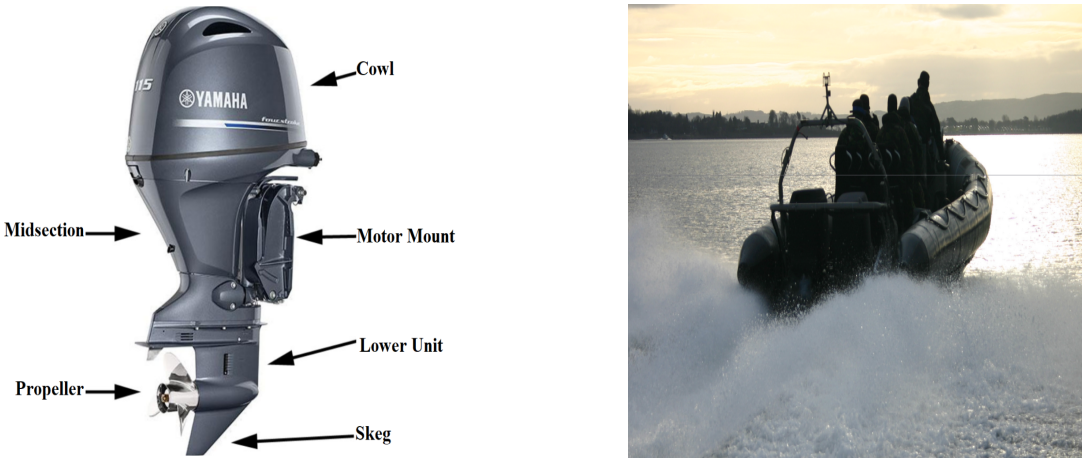

(a) **(b)**

Figure 1.1: High-Speed Boat Running on an Outboard Engine (a) Outboard Engine and (b) High-Speed-Boat (International, 2006)

1.2 Outboard Marine Propulsion System

The propulsion system of a boat is an assembly of components to drive boats based on rotary motion. The outboard engine can be divided into six subsystems based on their functions: the mechanical drive system, the swivel bracket system, water intakes, the propulsion system and the exteriors, as shown in Figure 1.2.

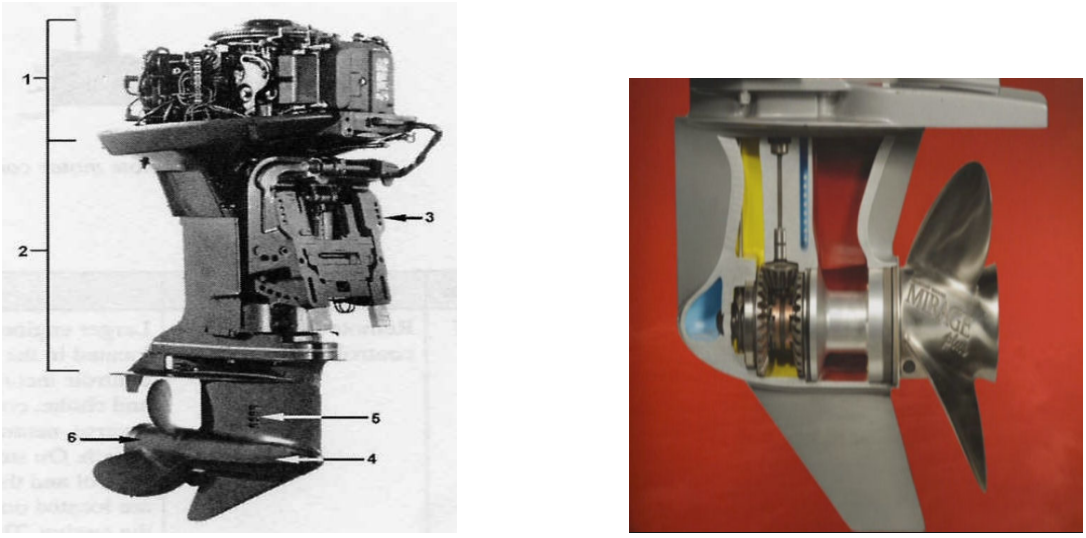

(a) (b)

Figure 1.2: Outboard Propulsion System with (a) Engine Parts and (b) Marine Propeller (Courtesy of Outboard Marine Corporation, 2001)

In Figure 1.2 (a), parts 1 and 2 represent the Mechanical drive system. Part 3 is the Swivel bracket system, part 4 is the Gearbox, part 5 is the Water intakes, and part 6 is the outboard marine Propeller.

The mechanical drive system includes the engine and transmission shafts to generate the kinetic energy. A swivel bracket system is the supporting and turning base and unloads the thrust from the propeller with its clamp fixed at the boat's stern. The sea water enters at this point and flows through the engine for cooling purposes. The exteriors are the covers, connections and decorative pieces. The gear box and propeller make up the propulsion system. The most critical propulsion systems is the propeller, which produces the power needed to turn the main engine as shown in Figure 1.2 (b). Its configuration involves a mechanism to push water, with the resultant reaction propelling the boat forward. It plays a great role in the fuel efficiency, thrust, torque and overall efficiency improvement. Due to its role in the performance of the boat, it is necessary to predict the performance of the considered propeller. Therefore, the most preferred methods for the prediction are the RANS approach and open water series method. The latter is also known as the Wageningen-B-screw propeller series because of its low cavitation risk (Benini, 2004). Oosterveld et al. (Oosterveld & Van Oossanen, 1975) made a detailed regression analysis for the performance characteristics using Wageningen-B-propeller series. Later, Newton Rader developed a propeller series to analyze the propeller performance characteristics data for the high-speed boats. The range of pitch-to-diameter ratios was found to be 1.0 to 2.0 for a three-bladed propeller (Newton-Rader, 1961). Most of the research on marine propellers focused

on impact of variation of geometric parameters such as angles, blade thickness, chord length, camber, pitch, and diameter. In these studies, propeller performance and associated instabilities were predicted. However, not much research has been done on the impact of pitch-to-diameter ratio, number of blades and rotational speed. Also, previous work has focused on propeller performance characteristics using methods such as vortex lattice method, unsteady propeller design method and a multi-objective numerical optimization approach based on boundary element method to solve blade cavitation. Using these methods, the problem has not been effectively solved because of the complexity of motion of high-speed boats.

Although, there has been research on open water propeller performance, it is necessary to investigate the performance improvement of the high-speed boat running on an outboard engine. A study of the open water propeller performance based on the geometrical aspects is needed in order to obtain an efficient propeller of an outboard engine. There is, therefore, need to improve performance of the high-speed boat for the local market in order to enhance operations in blue water for support in short distance operations, border security operations, international peacekeeping and disaster relief (Haynes, 2014).

1.3 Problem Statement

Propeller inefficiency is a major problem in marine industry since the development of high-speed boats and the inefficiency can largely be traced to blade cavitation. This has been found to reduce the performance of the propeller as it leads to an eroded and corroded blade surface, loss of thrust and induced vibration. The world is facing an environmental, social and economic problem due to harmful emission, high power consumption, fuel wastage and boat accidents (Erik, And, & Henthorn, 2004; Assessment and Standards Division Office of Transportation and Air Quality (ASDOTAQ), 2008; Zhao, Yang, Wan, & Kiang, 2015; Kuzminski & Jackivicz, 1972). The unburned fuel in boats using an outboard engine increases from 31.25% to 54.7% when the boat cruises at high speeds (Kuzminski & Jackivicz, 1972). A boat engine running on low speed of less than 600 rpm showed a fuel wastage of above 10%. Fuel wastage and exhaust emission increase environment pollution by 20% (Gusti & Semin, 2016).

Inefficient propeller and blade cavitation have existed since the screw propeller was first introduced to the marine environment. Since the second world war, propeller performance has been investigated increasingly through model tests in towing tank and cavitation tunnel (ITTC, 2011; H. A. Kutty & Rajendran, 2008). Cavitation was also

found to affect the propeller performance and it is defined by cavitation number (σ_0) (ratio of the static to dynamic head of the flow). It was found that as σ_0 decreased in value, cavitation took more negative effect on propeller performance characteristics. Cavitation reduced the propeller efficiency by 9.5% as the value of σ_0 decreased (Johnson, 2011a; Newton-Rader, 1961; Favacho et al., 2016; Kehr, 1994). It was also found that when cavitation covered 20 to 25% of blade section resulted in reduction of both thrust and torque. As thrust decreases more rapidly than torque, it reduced the propeller efficiency (Basumatary Jahnabi, Wood, 2017).

In 2002, it was reported that 21% of high speed boats accidents involved injury, 48% of accidents involved property damage only and 25% death due to propeller damage (Bruce, Ted, & Maxim, 2006). Since sufficient work has not been done to improve the propeller performance in outboard engines, efficient propulsion system for high-speed boats are still in great demand. This is due to its wide application in water for support in marine security operations and disaster relief. There is a need to improve performance of fast watercraft running on an outboard engine to improve the propeller efficiency which is the main objective of this work.

1.4 Objectives

The general objective of this research is to improve the performance of high speed boat's propulsion system for operating a high speed water craft by using computational fluid dynamics. This general objective will be achieved through the following specific objectives:

1. To develop a propeller model for the high-speed boat running on an outboard engine.
2. To study the influence of propeller geometry such as blade number, and pitch-to-diameter ratio on the propeller performance.
3. To investigate the influence of rotational speed (rpm) on the propeller performance.

1.5 Justification

Utilization of outboard engine is increasing in the high speed boats all over the world for maritime security, supporting in short distance operations, and international peace-keeping. The East Africa countries policy identify maritime transport as one of the infrastructure enablers of its social and economic pillars (Griffiths, 2005; Zainol &

Yaakob, 2016). Sustainable, affordable and reliable means of transport for all citizens is a key factor in the realization of the policy. Evidently, the improved propeller performance of high-speed boats running on an outboard engine ensure the affordability, sustainability and protection of the environment. An efficient propeller is one of the essential components of the propulsion system of the high-speed boats running on an outboard engine since it results in adequate open water propeller performance characteristics (thrust coefficient (K_T), torque coefficient (K_Q), and open water efficient (η_0)) (Eckhardt, 1955; Vesting, 2015). This also results in minimum power absorption, fuel consumption and improved efficiency. Moreover, an efficient propeller also provides additional environmental benefits like reduction of the harmful exhaust gas emissions (Egerton, Rasul, & Brown, 2007; G.A.Butcher, 1985; J.Porteiro Lopez Gonzalez, 2005). The ability to improve the outboard marine propeller performance for high-speed boats can lead to significant increase in profitability for the marine engine manufacturers to design efficient marine propellers. Lastly, this will also sustain economy of the marine engine and high-speed boat industries by reducing maintenance expenses that occur due to frequent replacement of outboard propellers.

1.6 Organization of the Thesis

The current chapter is the introduction to this research which gives a general highlight of marine propeller inefficiency and needs for propeller performance improvement of high-speed boats running on an outboard engine. The second chapter presents a review of researches that have been carried out on the open water marine propeller performance and performance evaluation methods associated with the high-speed boats. Chapter three outlines the numerical set-up and method used to establish the performance parameters of an outboard marine propeller. Chapter four presents and discusses the results obtained from a computational fluid dynamics (CFD) simulation. Chapter five includes the conclusions deduced from the determined performance parameters and recommendations for further research to be carried out to make an outboard marine propeller reliable.

CHAPTER TWO
LITERATURE REVIEW

2.1 Overview

The outboard engine is considered as one of the typical modern propulsion systems being used in high-speed boats. This propulsion method is not as popular as the water jet usually used in fast craft but is competitive in certain operating conditions. The tendency to use outboard propulsion is increasing, due to the high performance, lower cost, simple installation, reduced fire risk, lighter weight and higher speed. The lack of an efficient propulsor is the biggest weakness of high speed crafts as highlighted by various researchers (Basumatary Jahnabi, Wood, 2017). The main cause of this as shown by Reynolds (Asimakopoulos, 2016) and Barnaby (S. Barnaby, 1897) is propeller blade cavitation. Propeller blade cavitation is a phenomenon which begins when a disturbance creates a low-pressure area in the water flow. As speed increases, the low pressure intensifies enough to vaporize (boil) some of the surrounding water. When the vapor bubbles approach a high pressure area, they collapse, releasing energy and causing damage. Cavitation is also caused by a disturbance of the water flow in front of the propeller. Cavitation also results from an irregularity in the boat bottom or gearcase, and a misplaced transducer or speedometer pickup (RINA, 2011). Cavitation affects the propeller performance as it leads to reduction in the thrust and efficiency as illustrated in the Figure 2.1.

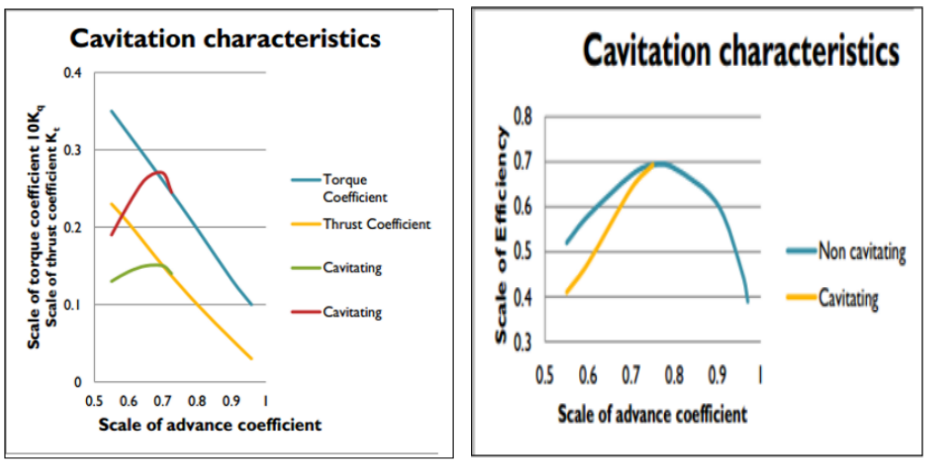

(a) **(b)**

Figure 2.1: Effect of Cavitation on Propeller Performance (a) Thrust and Torque Coefficients and (b) Open Water Efficiency (RINA, 2011)

Cavitation leads to excessive vibration, noise, and further blade erosion. Cavitation can also decrease the serviceability, and durability of the high-speed boats. In addition, it

causes high fuel consumption resulting in high harmful gaseous emissions which are hazardous to the environment (Zhao et al., 2015).

In order to improve the performance of the outboard engine in high-speed boats, various concepts have been developed. Different researchers have put much emphasis on modeling the propeller parts geometry to improve the boat performance. The marine propeller configuration involves a mechanism to push water, with the resultant reaction propelling the boat forward. It also has the ability to improve the propeller efficiency, thrust, and torque and consequently the fuel efficiency. This chapter presents a review of research works that have been done by various researchers concerning parameters affecting the performance of marine propulsion system and also concepts that are useful in modeling the blade. The main focus is on the parameters that affect the marine propeller performance as well as to identify the gaps in the literature that need to be addressed.

2.2 Marine High-Speed Craft

The design and safety of high-speed craft is regulated by the High Speed Craft Codes of 1994 and 2000, adopted by the Maritime Safety Committee of the International Maritime Organization (IMO) (The Maritime Safety Committee, 1994). Savitsky et al. (Savitsky Daniel & Ward, 1976) defined high- speed vessels as crafts that can travel at a sustained speed equal to or greater than 35 knots with bursts of high speeds of 40-60 knots. Froude number allows for another way to hydrodynamically classify ships. Naval architects use the Froude number when studying the interaction of water's free surface and hull. High speed vessels are typically defined by Froude number greater than 0.4 which at this speed range the crafts weight is almost entirely supported by dynamic forces. A high-speed craft (HSC) shown in Figure 2.2 is a vessel called a fast boat or fast ferry for civilian use and patrol craft for military purposes. A vast increase in high speed crafts has drawn considerable interest for both ship owners and naval architects. This due to existing needs in the field of fast transport of light and expensive cargo, and passengers for marine transportation. The high speed function also gives advantages to boats which are designed to be used for a surveillance and patrol in maritime area at open sea(International Towing Tunnel Commettee (ITTC), 1993).

Figure 2.2: Example of High-Speed Craft (HSC) (Haynes, 2014)

Currently, high-speed boats use either sub-cavitating (propeller operate at speed below 25 knots), super-cavitating (propeller operates at speed above 30 knots) and surface-piercing or waterjet propulsors due to their good efficiency as shown in Figure 2.3.

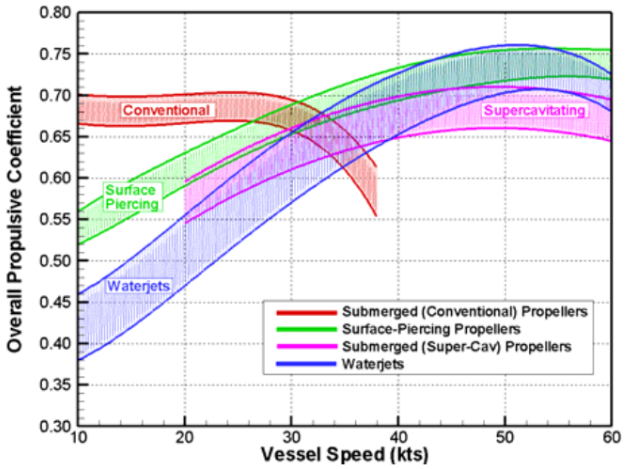

Figure 2.3: High-Speed Marine Vehicle Propulsors Performances (Am et al., 2005)

Am et al. (Am et al., 2005) developed the propeller blade profile that have the efficiency characteristics of conventional submerged sub-cavitating propellers at low and intermediate speeds but can transition to a super-cavitating mode for high speed operation without encountering thrust breakdown.

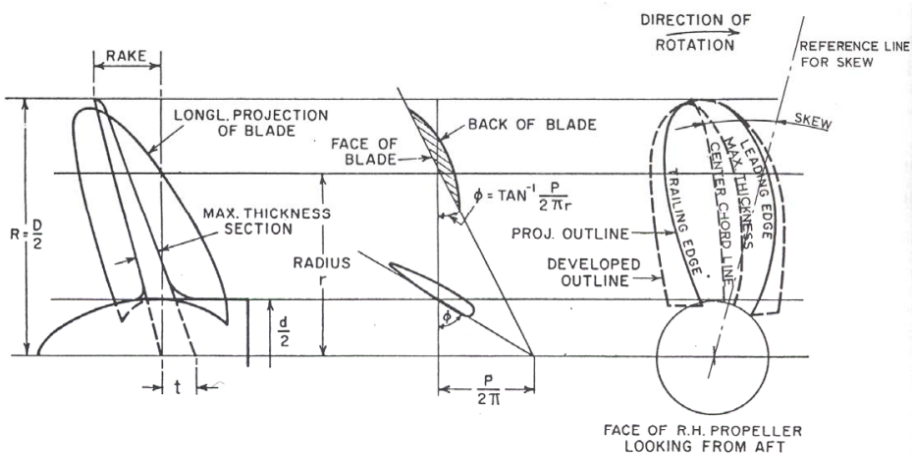

(a)

Diameter D Pitch ratio $= \dfrac{P}{D}$

Pitch P Blade thickness ratio $= \dfrac{t}{D}$

No. of blades 4 Pitch angle $= \phi$

Disk area = area of tip circle $= \dfrac{\pi}{4} D^2 = A_O$

Developed area of blades, outside hub $= A_D$

Developed area ratio $= DAR = \dfrac{A_D}{A_O}$

Projected area of blades (on transverse plane) outside hub $= A_P$

Projected area ratio $= PAR = \dfrac{A_P}{A_O}$

Blade width ratio $= BWR = \dfrac{\text{Max. blade width}}{D}$

Mean width ratio $= MWR = \dfrac{A_D / \text{length of blades (outside hub)}}{D}$

(b)

Figure 2.4: Parameters of Propeller Blade Section (a) Propeller Blade Section and (b) Basic Propeller Blade Section Definition (A.H.Techet, 2004)

The new design retained the same skew, chord, rake and span wise loading as the parent propeller in Figure 2.4.

The Propellers with these new sections were designed based on operational requirements at multiple speeds. The result showed that a new blade shape (S-shaped) section had the pressure surface and suction side completely enveloped by a cavity at high speeds. It was also found that at high speeds, super-cavitating propeller begun to cavitate either at their leading edge due to angle of attack fluctuations, or in the middle of the suction face due to the low pressure.

Young-Zehr Kehr (Kehr, 1994) designed a new series propeller for high-speed crafts with an expanded blade area ratio (ratio of the total area of the blades divided by the total area of the propeller) of 1.0. Experimentally, the new series propeller was

compared with the Newton- Rader series usually utilized for high-speed crafts. The Newton–Rader series holds a relatively limited set of twelve, three-bladed propellers proposed for high-speed craft. This series was designed to cover pitch ratios in the range 1.0 to 2.0 and expanded blade area ratios from about 0.5 to 1.0. The parent model of this series, had a diameter of 254 mm (10 in.) based on a design for a particular vessel as shown in Table 2.1. The variable parameters of the new series were blade number (three and four blades), pitch ratio (1.2, 1.4, 1.6, 1.8), cavitation number (0.5, 0.6, 0.75 and 5.5), and inclined propeller shaft angle ($0^0, 6^0, 8^0, 10^0$). This inclination is measured with respect to the horizontal axis when the boat is at rest.

The experimental results showed that the new series propeller in the study delivered a better performance than the Newton- Rader series. The results also showed that the efficiency of the propeller with new section was better than that of propellers with Newton-Rader sections at inclined shaft conditions. Moreover, the results showed that the three bladed propellers had a better efficiency than four-bladed propellers number. The experimental data also showed that there was a significant negative effect on the performance of propellers when the pitch-to-diameter ratio increased as the cavitation number decreased. From the Table 2.1 Z is the blades number, A_E/A_O is the expanded

Table 2.1: Newton-Rader Series Specification (Carlton John, 2012)

Series	*Number of propellers in series*	*Range of parameters*			*D (mm)*	*r_h/R*	*Cavitation data available*	*Notes*
		Z	A_E/A_O	P/D				
Wageningen B-series	≃120	2–7	0.3–1.05	0.6–1.4	250	0.169	No	Four-bladed propeller has non-constant pitch dist
Au-series	34	4–7	0.4–0.758	0.5–1.2	250	0.180	No	
Gawn-series	37	3	0.2–1.1	0.4–2.0	508	0.200	No	
KCA-series	≃30	3	0.5–1.25	0.6–2.0	406	0.200	Yes	
Ma-series	32	3 and 5	0.75–1.20	1.0–1.45	250	0.190	Yes	
Newton–Rader series	12	3	0.5–1.0	1.05–2.08	254	0.167	Yes	
KCD-series	24	3–6 (mainly 4)	0.587 Principal 0.44–0.8	0.6–1.6	406	0.200	Yes	Propellers not geosyms
Meridian series	20	6	0.45–1.05	0.4–1.2	305	0.185	Yes	Propellers not geosyms

area ratio, P/D is the pitch-to-diameter ratio, D is the propeller diameter and r_h/R is the radius ratio.

High-speed boats are classified into two categories which are an air-supported and displacement type. Air supported crafts include air cushion vehicles (ACV), surface-effect ships (SES) and foil supported craft (FSC) such as hydrofoils and jetfoils. Displacement type vessels include conventional monohull, catamaran, trimaran, small water plane area twin hull (SWATH), and air lubricated hulls. Each type of craft has

its unique characteristics such as form of hull shape and mode of power transmission. They all suffer from the common problem of limited payload and sensitivity to wind and sea state. Besides, there are vessels with a design speed corresponding to a Froude number above 0.45, primarily designed for short distance services such as public transport of passengers and vehicles. An outboard engine, inboard/outboard drive, or inboard diesel waterjet can power the high-speed watercraft (ITTC, 2011; Yousefi, Shafaghat, & Shakeri, 2013). The improved performance of the high speed boat for the local market is to enhance the operations in seas or lakes for support in short distance operations, border actions, and international peacekeeping or disaster relief (Haynes, 2014; A. Baquero and A.Haimov, 1999).

2.3 Marine Propeller System

Marine propeller design is used to obtain a blade geometry which meets the requirements determined by the operating condition by using various design methods (Carlton John, 2012; J. E. Kerwin, 2013). The optimization of the outboard propeller is to provide the maximum thrust for the minimum torque at a specific rotational velocity (rpm) with a particular boat speed (Wan, 2014). Initially, propeller design intended to achieve the highest efficiency. However, cavitation effect came into focus meaning the propeller design had to consider the two aspects; efficiency, and cavitation as found in the work of Subhas et al. (Subhas, S, V F Saji, S. Ramakrishna, 2012).

2.3.1 Propeller Selection Criteria

Choosing the right propeller is crucial in determining the performance of the outboard engine (Johnson, 2011b). Propeller choice can increase the boat top speed from 5 to 10 knots. It also has a direct effect on acceleration, cornering, pulling power and fuel economy. Some boats may require change of propellers for different activities, such as high speed cruising, water skiing, or carrying heavy loads. Using the wrong propeller in any of these applications will not only affect performance, but could also cause engine damage (Barry, 2005). There are also many types of propeller systems in operation. The right hand fixed blade propeller is still common. Meanwhile, development in controllable pitch propellers, contra-rotating propellers, multi-blade propeller systems, twin, triple and quadruple propeller sets, pod propulsion units, Kort nozzle systems and azipod systems have also taken market share in both commercial and boat construction (Ekinci, 2010).

The propeller is a key part used as a prime mover for water crafts. Furthermore, utilizing an outboard propeller in high speed boats avoids any other damages such higher

fuel and power consumption, and environmental pollution. This was found in the work of Tani et al. (Tani et al., 2017) while analyzing the flow around propeller and performance characteristics (the thrust and torque coefficient, and efficiency and their variations with the advance coefficient). Currently, with access to superior hardware and software, it is possible to model the complex fluid flow problems like marine propeller flow and open water performance.

Marco et al. (Marco, Mancini, Miranda, Scognamiglio, & Vitiello, 2017) performed an experimental and numerical analysis of marine propeller. The study was carried out to know the open water performance and evaluate the velocity field in the propeller wake. The experimental results showed that the tip vortex was identified by turbulence level peaks in the flowfield, whereas in computation results its position was identified with the outmost stream wise wake node line. It was also found that the open water propeller performance was in good agreement with the experimental results. However, pressure distribution needed to be illustrated in order to study the effect of advance coefficient on the fluid flow around the propeller blade sections.

Burger et al. (Burger, John E. Burkhalter, Roy J. Hartfield, Robert S. Gross, & Ronald M. Barrett, 2007) developed also the propeller performance analysis program and integrated it into a genetic algorithm to investigate the feasibility of designing propellers. It was found that the optimized propeller had favorable performance but circulation distributions were less smooth when compared to multi-objective optimizations. However, for the free wake propeller model, the lower advance coefficient needed to be studied to improve the hydrodynamic propeller performance prediction. Watanabe et al. (Watanabe, Kawamura, Takeoshi, Maeda, & Rhee, 2003) applied unstructured grid technique to study the flow around the marine propeller. The comparison of his study with the experimental data was good for both steady and unsteady conditions.

Motley et al. (Michael R. Motley, 2017) investigated a reliability-based global design of self-adaptive marine propellers operating under a range of steady loading conditions, using a Nelder-Mead constraint based optimization technique. An optimized propeller was found to reduce the load variation by approximately 10%, potential flow by 2.3% on the back side and 9.7% on the face side. It also increased the total efficiency by approximately 0.3%.
Rag (Coast, Auxiliary, & Manual, n.d.) investigated the effect of propeller selection on the propeller performance using an experimental analysis. It was found that selecting the right propeller for boat resulted in a good performance in terms of efficiency, fuel

consumption, and speed. The author found that the wrong choice of propeller damaged propeller and caused a drop in top speed by 13% and 37% in acceleration while optimum fuel miles were reduced 21%. However, the author advised that to get the maximum efficiency from the engine, the pitch should be matched to engine power, gross weight and intended use of the boat.

2.3.2 Geometrical Parts of Outboard Propeller

Marine propeller is a set of identical twisted blades, spaced evenly around a hub. Most propellers have a splined bushing in the hub that mounts on the outboard. Figure 2.5 bellow shows an example of marine propeller used in outboard engine (Johnson, 2011b; E.Slater & John, 1988).

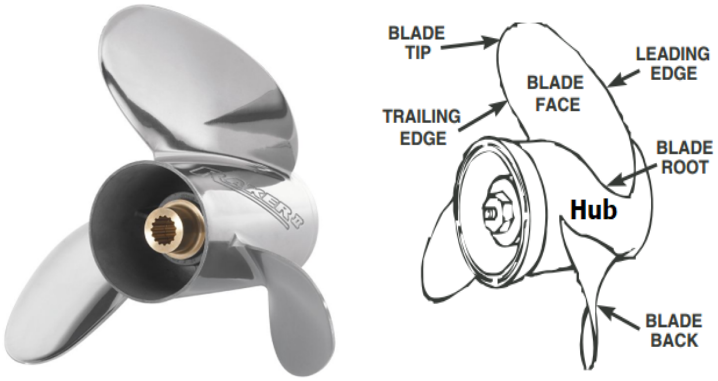

(a) **(b)**

Figure 2.5: Outboard Marine Propeller for High-Speed Boats (a) Picture of Common Outboard Propeller (b) Basic Marine Propeller Terms (Johnson, 2011a)

The marine outboard propeller parts include; the boss of a propeller (hub) which is the solid center disc, to which the propeller blades are attached. The propeller blades are the twisted fins or foils that project out from the hub. It is the action of the blades that drives a boats through the water. It has two opposite sections which are blade face and blade back. The blade face is the high-pressure side, or pressure face of the blade. It is the side facing aft, the side that pushes the water when the boat is moving forward. The rear of the blade is the low pressure side or suction face of the blade, the side facing ahead. Moreover, the blade has other important part such as the blade root which is the point at which the blade is attached to the hub and the blade tip, the extreme outermost edge of the blade. At the blade tip, leading edge is the edge of the blade that cleaves the water and trailing edge is the edge from which the water streams away (Johnson, 2011b; Propellers, 2009; Michigan Wheel Engineering, 2000). Kiam

and Wai (Kiam Beng Yeo and Wai Heng Choong, 2014) developed a marine propeller geometry characterization using 3-D scanning and computer aided design. Computational fluid dynamic analysis was used to investigate marine propeller hydrodynamic performance. An outboard marine propeller was utilized to demonstrate the feasibility of the study. It was found that the geometric properties can be successfully characterized. The characterizing process was concluded successfully by presenting the obtained geometry parameters into the standard propeller drawing. However, this study did not consider the effect of propeller blade cavitation.

2.3.3 Marine Propeller Materials

Materials used for the marine propeller of today's propulsion system include Aluminum, stainless steel, non-metallic composite reinforced plastics or bronze (often an alloy called NiBrAl). Aluminum propellers are the most common. Aluminum provides a good balance of cost, performance and are suitable for the widest range of applications since there are so many models available. Stainless steel propellers offer the highest performance and best durability but are the most expensive. Composite and plastic propellers are generally used for emergency situations (Choong, Yeo, Tamiri, Tze, & Teo, 2013). Table 3.1, shows the comparisons of materials used in marine propellers.

Table 2.2: Comparison of Materials for Marine Propeller (Choong et al., 2013)

Materials	Weight	Flex	Repair	Cost
Composite Boat Propeller	Least	Little	Not Possible	Least
Aluminum Boat Propeller	Medium	Little	Easy	Medium
Stainless Steel Boat Propeller	Greatest	Least	Difficult	Greatest

2.4 Marine Propeller Performance Characteristics

A propeller is normally fitted onto the lower unit of an outboard engine where it runs in water that has been disturbed by the boat as it moves ahead. The performance of the propeller is thus affected by the boat hull to which it is fitted. Hence, in order to determine the performance characteristics of a propeller unaffected by the boat to which it is fitted, it is necessary to make the propeller operate in open water (uniform flow) (Rawson & Tupper, 2010). Therefore, some of the parameters that can affect the performance while designing are subdivided into two categories, that is, open water characteristics which consist the forces and moments produced by the propeller. Secondly, propeller-hull interaction characterization which can be considered in two

separate categories: bearing forces which comprises the forces and moments transmitted through the shafting system and hydrodynamic forces which involves the forces experienced by the boats that are transmitted through the water in the form of pressure pulses (Burrill, 1944; John, n.d.).

2.4.1 Open Water Propeller Characteristic

The forces and moments produced by the propeller are expressed based on non-dimensional characteristics. These non-dimensional terms that captures the general performance characteristics are established using dimensional analysis (Rawson & Tupper, 2010; Chittaranjan Kumar Reddy, 2015). Thrust (T) and Torque (Q) can be represented by the following functions depending upon the physical quantities involved as shown by Techet et al (A.H.Techet, 2004)

$$T = f_1(\rho, D, V_a, N, \mu, p_o - e) \tag{2.1}$$

and

$$Q = f_2(\rho, D, V_a, N, \mu, p_o - e). \tag{2.2}$$

where, ρ is the density of the fluid, D is the propeller diameter, V_a is the speed of advance, N is rotational speed, μ is viscosity of the fluid and $p_o - e$ is the static pressure of the fluid at the propeller station.

Therefore, using the dimensional analysis open water propeller characteristics (thrust coefficient(K_T), torque coefficient (K_Q), and open propeller efficiency(η_o) and plotted with respect to the advance coefficient (J)) are given in the Equations 2.3 to 2.6 as shown in (A.H.Techet, 2004).

$$K_T = \frac{T}{\rho N^2 D^4}, \tag{2.3}$$

$$K_Q = \frac{Q}{\rho N^2 D^5}, \tag{2.4}$$

$$J = \frac{V_a}{ND} \tag{2.5}$$

The open water efficiency of the propeller is the ratio of useful power produced by the propeller, the thrust horsepower (THP), to the input shaft power, the delivered horsepower (DHP):

$$\eta_o = \frac{THP}{DHP} = \frac{TV_a}{2\pi NQ} = \frac{K_T \rho N^2 D^4 V_a}{2\pi N K_Q \rho N^2 D^5} = \frac{K_T}{K_Q} . \frac{V_a}{2\pi ND} = \frac{K_T}{K_Q} . \frac{J}{2\pi} \tag{2.6}$$

where: D is the propeller diameter, N is the rotational speed, V_a is the speed advance, ρ is the density of the fluid, μ is the dynamic viscosity of the fluid and g is the gravity. In addition, the details of this derivations are shown in Appendix A.

Several researchers have investigated the open water performance of the marine propellers using computational fluid dynamics. Among them, Sanchez-Caja et al. (Sánchez-caja, 2015) used RANS code FINFLO to study the scale effects on performance coefficients for a contracted-loaded tip (CLT) propeller with different end-plate geometries. The authors used SST k-ω as a basic turbulence model for the study. They used a special procedure to generate the computational grids in order to minimize computational errors. The results showed that the predictions of thrust and torque were decreased by 2.0% and 1.5 % compared to the experimental values respectively. However, the refined grid needed to be adopted at the blade tip for better prediction of the tip vortex flow.

Bertetta et al. (Bertetta, Brizzolara, Canepa, Gaggero, & Viviani, 2012) presented an experimental and numerical analysis of unconventional CLT propeller. Two different numerical approaches, a potential panel method, and RANS solver were employed. The open water performance characteristics results of both methods were compared. The results showed that thrust coefficient reduced by 1.45% in the case of the panel method, 4.3% in the case of RANS while torque coefficient was reduced by 1.4% and increased by 1.5% in case of RANS solver and panel method respectively. However, a fine resolution of the RANS discrete volume mesh at the tip and root of the blades is required in order to improve the open water propeller performance characteristics.

Chau et al. (Chau, Kouh, Wong, & Chen, 2005) developed a propeller design method based on a vortex lattice algorithm to optimize the shape and efficiency. Two techniques were used to improve the efficiency up to 23%. The first code was sequential unconstrained minimization techniques for minimizing the torque coefficient. The second was a modified genetic algorithm to maximize efficiency. Blade'chord and thickness distributions were considered as design variables. The results showed that the efficiency improved by 13% according to objective of the author and the torque coefficient decreased by 15% . However, the efficiency needed to be improved up to 23% in order to reach the desired propeller performance.

Numerically, Fang et al.(Zhu & Fang, 2012) and Belhenniche et al. (Belhenniche, Aounallah, Omar, & Çelik, 2016) investigated the cavitation and hydrodynamic per-

formance of the propellers to predict propeller performance characteristic. The vapour volume fraction on the back side of propeller blade was predicted to show the effect of cavitation number. The authors used viscous multiphase flow theories based on RANS approach. The advance coefficient (J) and cavitation number (σ_n) were used as variables to validate the results. It was found that for the high value of advance coefficient, the cavitation was relatively weak and had little effect on the hydrodynamic performance whereas at the small value of advance coefficient the cavitation was strong. The results also showed that the increase of cavitation number improved the propeller performance characteristics. However, The effect of cavitation number needed to be studied in order to investigate the propeller performance characteristics by considering the propeller design parameters such as blade number, pitch-to-diameter ratio, and blade area ratio.

2.5 Parameters that Affect the Marine Propeller Performance

Performance characteristics of a marine propeller are affected by different factors. In the search to improve the open water propeller performance, various researchers have embarked on studies of different parameters such as geometric parameters and flow field around the propeller.

Design geometric parameters influencing the performance of the propeller include the diameter, pitch, pitch- to-diameter ratio, rotation speed, blade number, skew angle, blade area ratio, blade shape and blade thickness.

2.5.1 Effect of Pitch to Diameter Ratio (P/D)

The pitch diameter ratio (P/D) expresses the ratio between the propeller's pitch (P) and its diameter (D). The pitch is the distance the marine propeller propels itself forward through the water per revolution as shown on Figure 2.6 (a). As the pitch can vary along the blade's radius, the pitch diameter ratio is normally related to the pitch at 0.7R, where R = D/2 is the propeller's radius. Pitch is also determined as a nominal pitch in the relationship between propeller radius and pitch angle shown in Equation 2.7 (Carlton John, 2012; Greco, Leone, Testa, Salvatore, & Mauro, 2011). Propeller pitch is similar to the angle of attack in a hydrofoil as shown in Figure 2.6 (b) and the blade section of the propeller corresponds to a foil section. The foil characteristics change with the angle of attack while the blade characteristics vary with pitch angle (Ghasseni & Ghadimi, 2011).

$$P_m = 2\pi r tan\phi, \tag{2.7}$$

where, P_m is the nominal pitch, r is the hub radius and ϕ is the angle of attack.

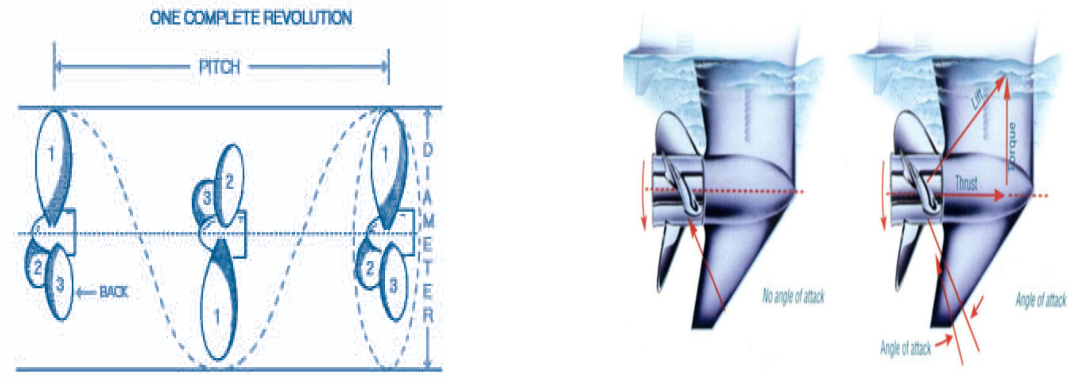

(a) **(b)**

Figure 2.6: Marine Propeller Pitch (a) Theoretical Marine Propeller Pitch and (b) Pitch Angle (Carley, Reg & Gray, 2000)

The pitch of a propeller is also defined similarly to that of a wood or machine screw. It indicates the distance the propeller would "drive forward" for each full rotation. In reality since the propeller is attached to a shaft it will not actually move forward, but instead propel the ship forward. Therefore, the distance the boat is propelled forward in one propeller rotation will be less than the pitch. For high speed craft, pitch ranges from 9 inch to 24 inches. Typically, the blades are twisted and bent to guarantee constant pitch along the blades from root to tip. Often a pitch ratio will be supplied. This is simply the ratio of pitch to diameter, and typically falls between 0.5 and 2.5 with an optimal value for most vessels closer to 0.8 to 1.8. Pitch effectively converts torque of the propeller shaft to thrust by deflecting or accelerating the water behind as stated by Newton's Second Law of motion (Carlton John, 2012; MAN Diesel & Turbo, 2011).

Experimentally, Mashud (Mashud, 2002) investigated the theory of marine propeller selections. The author showed that the fundamental task in selecting a propeller was to choose a pitch and diameter that will generate the maximum thrust possible at normal operating speed without overloading the engine. It was found that large diameter, without pitch or angle of attack would not accelerate any water behind (astern). Similarly, ordinary blades with too much pitch would attempt to force more water behind more quickly than the engine can accommodate. It was also showed that increasing pitch, increased thrust but reduced the efficiency of the engine and propeller combination by slowing the engine. Moreover, too little pitch will not overload or slow the engine, it will not accelerate as much water astern and thus will not generate maximum possible thrust or speed (Favacho et al., 2016).

Kamarlouei et al.(Kamarlouei, Ghassemi, Aslansefat, & Nematy, 2014) designed a marine propeller to generate the thrust with lower torque, highest efficiency and reducing cavitation. The author used numerical method based on Blade Element Theory (BET) to get the thrust and analyze how it depends on the shape of the marine propeller. The parameters such as pitch ratio, blade area ratio and skew angle were used as the input variables to achieve the optimum propeller performance. It was found that various pitch ratios such as 0.4, 0.6, 0.8, 1.0, 1.2, and 1.4 used satisfied the propeller performance characteristics. The skew angle effect also showed its capacity to estimate the propeller efficiency in limitation of cavitation problem. This research did not consider blade number effect on propeller performance.

Wai et al.(Wai Heng Choong & Hau, 2014) investigated the marine propeller performance characterization through CFD to predict a three blade marine propeller performance characteristics. Five propellers with a pitch to diameter ratio values of 0.6; 0.8; 1.0; 1.2; and 1.4 were used for the computational flow analysis through RANS solver to compute the propeller performance characteristic at various advance coefficient (J). It was found that efficiency, torque, and thrust increased as the pitch diameter ratio increased. However, the effect of pitch ratio range above 1.4 needed to be studied for open water propeller performance.

M.Bernitsas et al. (M.Bernitsas, Ray, 1981) designed the Wageningen B-Series propeller to test the open water characteristics using the multiple polynomial regression analysis. The parameter such as number of blades, the blade area ratio, the pitch-diameter ratio and the advance coefficient were used as input variables. It was shown that the derived polynomials is valid for the pitch-diameter ratio varying between 0.5 and 1.4 for the Reynolds number of 2×10^6. It was also found that the thrust coefficient displayed a local maximum for high pitch-diameter ratio, high number of blades, low blade area ratio and low values of advance coefficient. However, the extremes of the above ranges were not considered in this research.

2.5.2 Effect of Number of Blades

The shape of the blades and the speed at which they are driven dictates the torque a given propeller can deliver. The primary effect that is to be avoided with propeller blade number selection is resonance, as the number of blades affects the frequency and strength of vibrations that occur during operation (Felli, Guj, & Camussi, 2008; Mashud, 2002). There is also a strong interrelation between diameter, blade area and blade number, with a greater diameter requiring fewer blades and a greater area requir-

ing more blades. An increase in propeller blade number can reduce sheet cavitation of the suction side due to a reduced load per blade, however it can increase root cavitation due to reduced clearance between each blade. It is recommended that the number of blades should be in the range of 2 to 6 blades to reduce the resonance (Carlton John, 2012; A. Baquero and A.Haimov, 1999).

Kiam et al. (Kiam Beng Yeo, Rosalam Sabatly & Hau, 2014) also investigated the effects of number of blade on marine propeller performance. Five propellers with number of blades from two to five were utilized for the computational flow analysis through RANS solver to investigate the propeller performance. It was found that the efficiency decreased as number of blades increased while torque and thrust increased. The results also showed that the increase in number of blades provided better flow velocity distribution on propeller blade section. However, the effect of diameter, pitch-to-diameter ratio were not considered in this work.

Wu et al. (Wu, 2010), investigated the effect of number of blades on propeller performance. Numerical simulation was used to study blade number effect on propeller blade performance and cavitation. The author tested propeller of blades number within the range of two to six. It was found that more number of blades increased thrust. The result also showed that less number of blades avoided cavitation and decreased thrust. The author concluded that, ideally, a good propeller has a large diameter, slow speed, low number of blades and high efficiency.

Boucetta et al. (Boucetta & Imine, 2016) investigated the open water performance of DTMB 4148 propeller with commercial CFD code FLUENT. The SST k-ω model was chosen for turbulence closure. Their investigation was focused on the effects of number, thickness and skewness of the blades on the open water performance. Based on the study, the authors concluded that among three, four and five blade configurations, four blades provide the best efficiency. Also, increase of thickness improved the efficiency while skewness of the blade improved the overall hydrodynamic performance. computational results of the effect of blade number was not in good agreement with the experimental results. However, the effect of blade number on hydrodynamics characteristic is needed to improve the propeller performance.

2.5.3 Effect of Propeller Rotational Speed

Rotational speed is the number of full turns or rotations of a propeller in one minute. High speeds are not efficient except on high speed vessels. For vessels operating under 35 Knots speed, it is usual practice to reduce rotational speed, and increase diameter,

to obtain higher torque from a reasonably sized outboard engine. For high speed boat, speed is ranging from 900 to 6000 rpm and from that it is possible to get the inflow velocity for a given advance coefficient (Newton-Rader, 1961; Wu, 2010; Casciani-Wood, 2014).

Harte et al. (Harte, Bose, Clifford, Roberts, & Davidson, 2011) investigated an application of paddle wheel propulsion in high speed craft to study the effect of rotational speed on propeller performance. Savitsky's planning method was used to estimate the resistance of the skiff and comparison of thrust coefficient at maximum and minimum revolutions. It was found that the trials on a paddle-propelled skiff demonstrated the possibility of propelling a surface craft at speeds more than 30 knots. It was also shown that at maximum revolution, the speed reached 35 knots and at minimum revolution, the maximum speed was about 46 knots. The result showed that the thrust coefficient decreased as the rotation speed increased. However, the effect of rotational speed needed to be studied in order to predict the propeller performance characteristics.

2.6 Effect of Flow Field Around the Propeller Blade

The flow around the propeller is complex due to its geometry and the combined rotation and advancement into water. Marine propeller is a very complex geometry, with variable section profiles, chord lengths and pitch angles, and in operational conditions it induces rotating flow (the inflow velocities onto the blade composed of the collective axial and rotational velocities and pressure field flows) and entails tip vortex (Sileo, Bonfiglioli, & Magi, 2006; Martínez-Calle, Julián González-Pérez & Balbona-Calvo, 2016).

In order to study the flow field around a marine propeller, Mosaad et al.(Mosaad M.,Mosleh M. & Yehia, 2017) and Husaini et al. (Husaini, Samad, & Arshad, 2004) provided complete computational guidelines using RANS method. The geometry creation, boundary conditions setup, turbulence modeling and solution parameters of the flow around rotating propeller were modeled. $K-\omega$ and $k-\varepsilon$ turbulence models of RANS solver were used to compare the propeller performance characteristic. The pressure field on the blades showed low pressure on the suction side and high pressure on the pressure side at advance coefficient of 0.5. It was found that the difference between computed and experimental results were less than 5% and 7% for thrust and torque coefficient using $k-\omega$ turbulence model and 7% and 10% for the same parameters respectively using $k-\varepsilon$. Therefore, the use of a $k-\omega$ model was shown to be efficient for propeller applications. However, the variation of advance coefficient

needed to be studied to investigate its effect on the velocity and pressure distributions on blade section.

Tian et al. (Tian & Kinnas, 2011) developed a numerical model to simulate the leading edge vortex (LEV) effect on propeller performance using the inviscid potential flow theory. LEV geometry and corresponding pressure distribution were compared with the result from inviscid finite volume method and RANS. It was found that the LEV model correlated with the results from RANS. However, Kutta condition of the leading edge detachment point needed to be studied around the propeller blade using RANS method.

Yang et al. (Yang, Zhou, Sciacchitano, Veldhuis, & Eitelberg, 2016) investigated propeller and inflow vortex interaction, vortex response and impact on the propeller performance. Propeller and flow vortex interactions were studied by stream-wise wingtip vortex impinging on a propeller. The result showed that tangential velocity of the vortex dominated the propeller performance while the axial velocity of the vortex had less impact on the propeller performance. It was also found that the propeller thrust and torque coefficients increased when the incoming vortex had the opposite direction of the propeller rotation, and vice-versa for the co-rotation vortex at a given advance ratio. However, the dynamic loading on the propeller was not considered in this research.

Gaggero et al. (Gaggero et al., 2017) designed a propeller for a high-speed craft using a multi-objective numerical optimization approach based on boundary element method. The efficiency was numerically investigated using RANS solver. The result showed that the design improved the propulsive efficiency, reduced blade cavitation. It was also found that the proposed approach was able to derive trade-off designs with high performance simultaneously concerning the flow field at suction and pressure side of the propeller blade. However, the fined volume meshes on the blade edges needed to be utilized in order to improve the propeller performance.

Giordini et al. (A. Giordani, F. Salvatore, 1999) carried out investigation of flow over DTRC 4119 propeller with a free wake model based on boundary integral surface panel method. The authors concluded that the prediction of velocity field in wake region was better when using this model. However, for better prediction of torque coefficient, proper viscous effects needed to be considered.

2.7 Propeller Performance Evaluation Methods

2.7.1 Experimental Methods

Experimental tests have been the method for the performance evaluation of propellers in both full and model scale settings. The former is achieved in ship trials and involves a non-uniform inflow wake due to the hull shape, while the latter can be done with or without the presence of a dummy hull model. Performance charts are produced by undergoing open water propulsion tests, conducted ideally in a deep-water basin, to avoid wall interferences. The tests are carried out by attaching a propeller on a moving carriage via a horizontal shaft, selecting a fixed rotational speed, and then conducting a number of runs, each with different forward speed until the desired range of advance coefficients J is achieved (ITTC, 2011; Brander, 2015).

Open water propeller performance tests, on the other hand, are conducted in Towing tank tunnels which have the ability to perform the towing and propulsion tests. Standard procedures require the propeller to be mounted on a dynamometer shaft, inflow speed (speed of the towing carriage) is set according to the desired advanced coefficient and rotation speed is set at a high value and kept constant. For studying the propeller performance in open water, a dynamometer shaft rotates the propeller model and measures thrust and torque. The results are illustrated in the open water curves (thrust and torque coefficients and efficiency as a function of the advanced number) as shown in the Figure 2.7 (Steen, 2014; Hanninen, 2015; M.Bernitsas, Ray, 1981; M.Faltinsen, 2006).

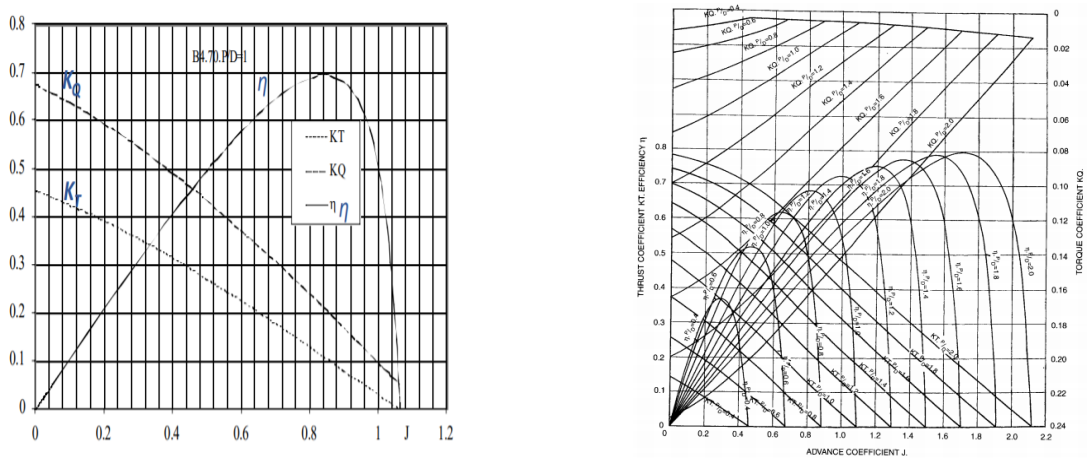

(a) **(b)**

Figure 2.7: Open Propeller Performance Characteristics Curves (a) K_Q,K_T and η_O Plot versus the Advance Coefficient and (b) K_Q, K_T and η_O Plot versus the Advance Coefficient for different P/D values (M.Faltinsen, 2006)

These evaluation methods have been implemented with wide acceptance by researchers and the industry, however, they involve a certain number of disadvantages. Firstly, satisfying flow similarity between the model and full scale is quite difficult, and thus various techniques are needed to transform tank test results. This demands a certain amount of empiricism and also allows for technique variation between different testing facilities. Furthermore, the time requirements and costs involved are not always feasible, which has led to a restricted amount of experimental data to become available. A combination of the above, and the complex geometry of propellers, which are tailor-made on a case-by-case basis, make the process quite restrictive and prone to errors (Ayris, 2016; H. Kutty & Rajendran, 2017).

An experimental and numerical investigation on hydrodynamic and aerodynamic characteristics of the planing trimaran was performed by Jiang et al. (Jiang, Sun, Zou, Hu, & Yang, 2017). The comprehensive series of viscous CFD simulations considering free-surface and 2-Degrees of Freedom (DOF) Ship Simulation motion of the hull was used. The calculated results were validated by comparing experimental and numerical data. The result showed that the calculated and experimental resistance increased from 2.99% to 14.66% as the Froude number increased from 3.16 to 5.87. In the numerical simulation, the total resistance increased up to the value of Froude number at which wave surface separated from the tunnel roof.

2.7.2 Numerical Methods

Numerical approach adopts a three dimensional (3-D) CFD simulation tested for various flow conditions. With rapid improvement of computational power, numerical methods have been a focal point for hydrodynamic analyses, including open water propeller testing. Both viscous and inviscid methods are constantly being developed and improved, becoming useful tools for initial design stages. Due to the high demands of viscous CFD in both time and computer resources, simplifications of the fluid flow can be introduced with acceptable accuracy. One such idealized scenario is potential flow (a flow which is irrotational, incompressible and inviscid) solvers. The time savings gained by replacing the Navier-Stokes equations and continuity equation with a simple linear equation, the Laplace equation, while still producing results close to experimental, have made such methods popular amongst naval architects (Salvatore, Greco, & Calcagni, 2011; Kajishima & Taira, 2017; Zhao Yaning, 2015; Yao & Zhang, 2018).

The numerical methods were carried out by using solvers such as Large Eddy Simula-

tion (LES) techniques, Detached Eddy Simulations (DES) and Direct Numerical Simulations (DNS), Reynolds averaged Navier Stokes (RANS) with different turbulence models, including one equation or two equations models. CFD methods had a quite significant impact as a useful tool for propeller design and performance analysis(Report, 1997).

However, in terms of practical propeller computations, as distinct from research exercises, the application of many of these methods are limited by the amount of computational effort required to derive a solution. As such, the RANS codes appear to have found most favour because the computational times are rather shorter than for the other methods (A.H.Techet, 2004; Omweri, Ondieki, & Hai-long, 2017). Most of the approaches have a number of common basic features in that they employ multi-grid acceleration and finite volume approximations. There are, nevertheless, a number of differences to be found between various practitioners in that a variety of approaches are used for the grid topology, cavitating flow modeling and turbulence modeling. In this latter context, there is a range of turbulence models in use, for example, k-ε, k-ω, Standard Wilcox k-ω, k-ε AKN, k-ε V2F and Reynolds stress models are frequently seen being deployed, with results from the latter two methods yielding good correlations (Menter, 1994).

Li et al. (Li Da-Qing & Carl-Erik, 2006) studied the influence of turbulence model on the prediction of model and full-scale propeller open water characteristics using RANS code fluent. Three models, SST k-ω, RNG k-ε and Realizable k-ε model were selected to study the scale effects of conventional and highly skewed propellers. The results showed that the performance predicted for all the models was fairly close to each other at model scale. Compared to experiments, the prediction error was less than 2% for K_T and less than 12% for K_Q. For the conventional propeller at full scale, the performance predicted by the SST k-ω model differs marginally from the two k-ε models. For the skewed propeller at full scale, there was notable difference in performance. The SST model predicted that K_T increased by about 5% with no change in K_Q. The k-ε models predicted a slightly decreased K_T (0.8%) and K_Q (5.6%). However, other RANS turburence model like Standard Wilcox k-ω, k-ε AKN needed to be considered.

Califano et al. (Califano & Steen, 2011) performed numerical simulations for a fully submerged marine propeller to study the effect of meshes set up on the open water propeller performance. The open water simulations were done by using CFD Fluent, based on RANS method. The meshing generated for the flow domain is fully unstructured on

the rotating domain and structured on the other region. The sliding mesh method was employed throughout the analysis to achieve rotation on the domain. The method used for numerical method managed to capture the flow simulation, with only 1% deviation for thrust coefficient. However, the base size meshes needed to be considered in order to improve the open water propeller performance.

Hong et al. (Hong & Dong, 2010) performed numerical study to determine the performance of ship propeller blade. Propeller DTMD4119 and CSSRC-TM0501 were taken as the study propellers, due to the availability of experimental data. The analyses were done using ANSYS Fluent, based on RANS model. The result showed that the numerical method results agreed with the experimental, with 6% maximum deviation. Moreover, the obtained results contained unexpected output, which was a sudden increase and decrease of the performance at certain advance coefficient. This was attributed to the boundary layer thickness that was not well predicted. However, other software using RANS solver needed to be utilized in order to improve the open water propeller performance.

Kawamura et al. (Kawamura, Watanabe, Takekoshi, Maeda, & Yamaguchi, 2004) investigated the influence of the turbulence model on cavitating and non-cavitating propeller open water characteristics using the commercial RANS code fluent. Computations for a conventional propeller were carried out using a two-layer RNG k-ε , standard k-ω and SST k-ω model. Thrust and torque coefficients were compared with measurements. The calculated torque coefficients were affected by turbulence model and the discrepancy between calculated and measured torque coefficients was smallest in the case of the standard k-ω model. However, the effect of the turbulence models such as Standard Wilcox k-ω, k-ε AKN, k-ε V2F were not considered in predicting the hydrodynamic characteristics.

2.8 Summary of the Gaps in the Literature

From the literature, the marine propeller performance is mainly affected by propeller design parameters. It has also been noted that propeller parts play a major role in predicting the propeller performance characteristics as well as fluid flow field around propeller. Therefore, the following gaps have been determined from the review:

1. Research has not be done to obtain an efficient propeller design for high-speed boats running on an outboard engine while reducing the propeller blade cavitation. Hence, there is need to improve the quality of propeller design in the cases of the flow fields distribution with regards to the risk of leading edge and the

pressure side.

2. Studies done on marine propeller performance have considered geometric configurations but there is minimum focus on pitch-to-diameter ratio and number of blades to improve the outboard propeller performance.

3. The use of outboard engine as an alternative propulsion for high speed boat remains a challenge due to the propeller blade cavitation which leads to an inefficient propeller. Thus, an investigation of the effect of rotational speed (rpm) on propeller performance is needed to get a marine propeller with the high-performance application.

4. An efficient marine propeller was shown to be obtained when the pitch is matching with the engine power, gross weight and intended use of the boat. Therefore, a study of pitch-to-diameter ratio greater than 1.4 is needed to improve the propeller performance.

5. An investigation of the parameters affecting the propeller blade cavitation for the performance of the high-speed boats running on an outboard engine needs further study to improve propeller performance.

6. The study of marine propeller performance has been directed towards usage of different types of meshes and turbulence model. Therefore, Standard Wilcox k-ω, k-ε AKN, k-ε V2F were not considered in predicting the hydrodynamic characteristics.

The aim of this work is to improve the performance of an outboard propulsion system for operating a high-speed water craft using CFD. The focus is on geometric parameters as listed in summary of gaps; number of blades, pitch-to-diameter ratio and rotational speed that highly influence the propeller performance. This improves marine propeller performance by reducing high fuel and power consumption. Hence, it is important to develop a model that will assist in improving the propulsion system performance for operating a small high-speed water craft. This creates a platform to identify the optimal parameter that guarantees improved propeller performance. The model also leads for reduction in fuel wastage, harmful emission and in a cost effective way.

CHAPTER THREE
METHODOLOGY

3.1 Introduction

This chapter presents detailed procedure used in the development and the selection of the outboard propeller and the methods used in the analysis. The propeller design is important and involves developing a blade geometry that operate effectively. Initially, propeller design aimed at the search of the highest possible efficiency. However, cavitation has become a key component in design consideration (J. Kerwin, 1986; J. E. Kerwin & B., 2001; John, 2012). The propeller performance optimization aims at providing the maximum thrust for the minimum torque at a specific rotational velocity (rpm) at a particular boat speed.

In this study, it is necessary to come up with an efficient propulsion system for a high-speed boat running on an outboard engine through investigating the open water performance propeller characteristics. The improvement of propeller efficiency is necessary to reduce power consumption by the engine. It is therefore necessary to investigate parameters affecting performance such as number of blades, pitch to diameter ratio, and rotational speed on propeller performance. An outboard propeller was modeled to study the influence of the parameters on performance of an outboard engine. The geometric model was created using Solidworks 2017 CAD and CFD analysis carried out using STAR-CCM+.

3.2 Geometric Modeling

3.2.1 Background

An outboard marine propeller was designed and modeled using computational fluid dynamic for open water propeller performance improvement. A computational geometry of the propeller was developed using CAD and imported to STAR-CCM+ which was used to perform flow simulation. Some of the key features of the STAR-CCM+ include ability to integrate with a CAD software and capability to analyze flow behaviour while simulations are running. It is also possible to apply a moving reference frame (MRF), to a region containing a moving part (CD-Adapco, 2016; Webster, 2015).

3.2.2 Design Model Set Up

A geometric representation of the outboard propeller was generated to test the open water propeller performance characteristics. The parameters for measurement of per-

formance included: propeller diameter, blade number, propeller pitch, pitch-diameter ratio and rotational speed. For the simplified sub-system model to be valid, it was important that all components be modeled adequately and their mating faces identified and coupled by appropriate interface models.

In SolidWorks, a model was created in which parts were associated to ensure that changes made to one part were automatically updated on other views (Chittaranjan Kumar Reddy, 2015; Mario Castro-Cedeno, 2015; Planchard, 2017). The OpenProp-SolidWorks.txt from the propeller design function was used as an input to generate the propeller blade structure in SolidWorks. After a propeller hub had been designed, a blade was created. Figure 3.1 (a) to 3.1 (d) show the hub and blade profile design. The sketch of hub was done on right plane as shown in Figure 3.1 (a) and then using revolve option the hub was generated as shown in Figure 3.1 (b). The blade profile was also sketched on reference plane which was taken at 30^0 to right plane as shown in Figure 3.1 (c), using extrusion option 5mm blade extrusion was performed and then using the flex operation, the blade was bent and twisted as shown in Figure 3.1 (d). Based on the geometry of the blade and hub, other blades were then generated by the Circular Pattern function in SolidWorks as shown in the Figures 3.2 (a) to 3.2 (c). The Table 3.1 shows propeller model specifications. These were the dimensions of a conventional outboard propeller used in high-speed boat by Johnson et al. (Johnson, 2011a). In this study, propeller blade profile was selected based on the results of the open water tests on an Open water propellers of the systematic B-series of MARIN, Wageningen, the Netherlands (John, 2012). With this series, propellers tested have varied parameters such as number of blades, blade area, pitch ratio etc. Based on these results and the requirement of the boat, the parameters were selected to obtain the suitable propeller design (Johnson, 2011a).

Table 3.1: Outboard Marine Propeller Specification (Johnson, 2011a)

Propeller components	**Dimensions**
Propeller diameter	0.304 m
Hub diameter	0.08 m
Hub length	0.15 m
Number of Blades	3
Blade thikness	0.005 m

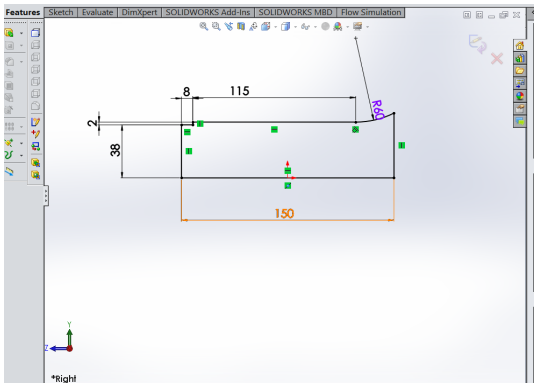

(a) 2D-Propeller Hub

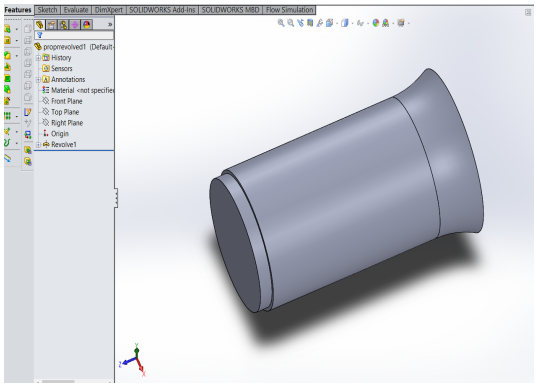

(b) 3D- Outboard Propeller Hub

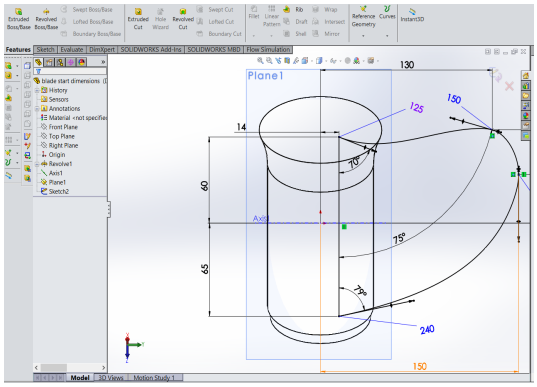

(c) 2D-Propeller Blade

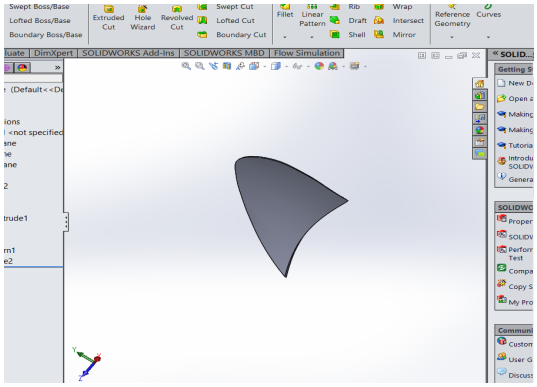

(d) 3D-Propeller Blade Twisted and Bent

Figure 3.1: Model of Outboard Marine Propeller Development

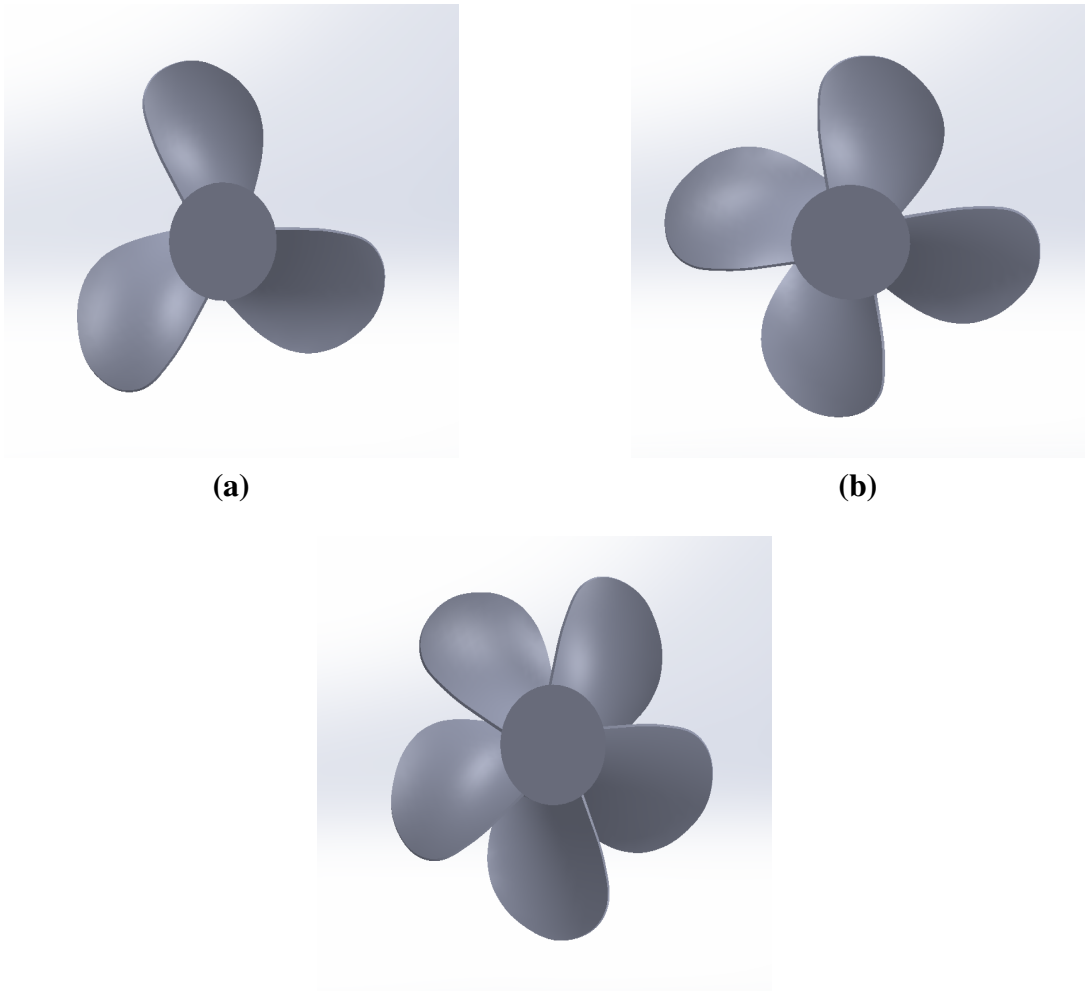

(a) **(b)**

(c)

Figure 3.2: Assembly of Outboard Marine Propeller with (a) Three blades (b) Four blades and (c) Five blades

The geometry of outboard propeller model shown in Figures 3.2 (a) to 3.2 (c) was modified by adding one and two blades but the surface (A_E) was maintained constant as shown in the Equation 3.1. These modifications followed also the chord law in Equation 3.2 found in the work of Carlton (Carlton John, 2012).

$$A_E = Z \int_{R_h}^{R_p} C_r dr = Z^* \int_{R_h}^{R_p} C_r^* dr \tag{3.1}$$

$$C_r^* = C_r \frac{Z}{Z^*} \tag{3.2}$$

After achieving the design model, the three-dimensional outboard propeller assembly was exported from SolidWorks 2017, with Initial Graphics Exchange Specification

(IGES) file extension, to STAR-CCM+ 9.06 for the simulation and analysis. Since the main area of interest was to ascertain the open water propeller performance characteristics of the outboard engine; the number of the blade, rotation speed and the pitch to diameter ratio were treated as variable parameters in the setup. However, water density particle and viscosity were treated as constant elements.

3.3 Set Up Parameters

In this study, before starting to calculate the open water propeller performance characteristics, the setup of all the parameters that are necessary for the simulation were established. The main stages consisted of computational domain set up, mesh generation and flow simulation.

3.3.1 Computational Domain Set Up

Flow features such as the velocities and energy dissipation, the pressure distributions, the turbulent kinetic energy, and vortex can be shown in the hydrodynamic analysis. In this work, Star-CCM+ version 9.06 with system requirements of Processor 2.4 GHz CPU with at least 4 cores per CPU was used for the flow simulation. Flow around the propeller blades was modeled as turbulent. The physical parameters were selected to facilitate accurately simulation of the physical model. In order to obtain approximate solutions in the turbulent flow, Reynolds-averaged Navier–Stokes equations 3.13 were used by averaging the physical parameters in the governing equation for a relatively long period of time to solve the time-averaged solutions in the turbulence model (Nath, 2012; Chittaranjan Kumar Reddy, 2015).

A computational domain is the surface plane surrounding a closed region around the marine propeller that used to simulate the CFD problem. Based on the conventional domains geometry found in Star-CCM+ 9.06 (Hai-Long et al., 2016), a computational domain was developed. Figure 3.3 shows the computational domain adopted for the RANS solver. The domain was composed of two cylindrical regions; a rotating region (small inner cylinder) containing the propeller and a static region (big cylinder) for the rest of the domain. The size of the domain determines how much volume surrounding the object of interest shall be included in the computation. Disregarding the computational time and computer power, increasing the domain will never result in a less accurate result. On the contrary, decreasing it, however, caused fatal errors due to reflections, and also impacted on the flow with a reversed flow. For this setup, a domain large enough was needed to avoid errors before a convergence test revealed the exact size needed (Omweri et al., 2017; Yao & Zhang, 2018).

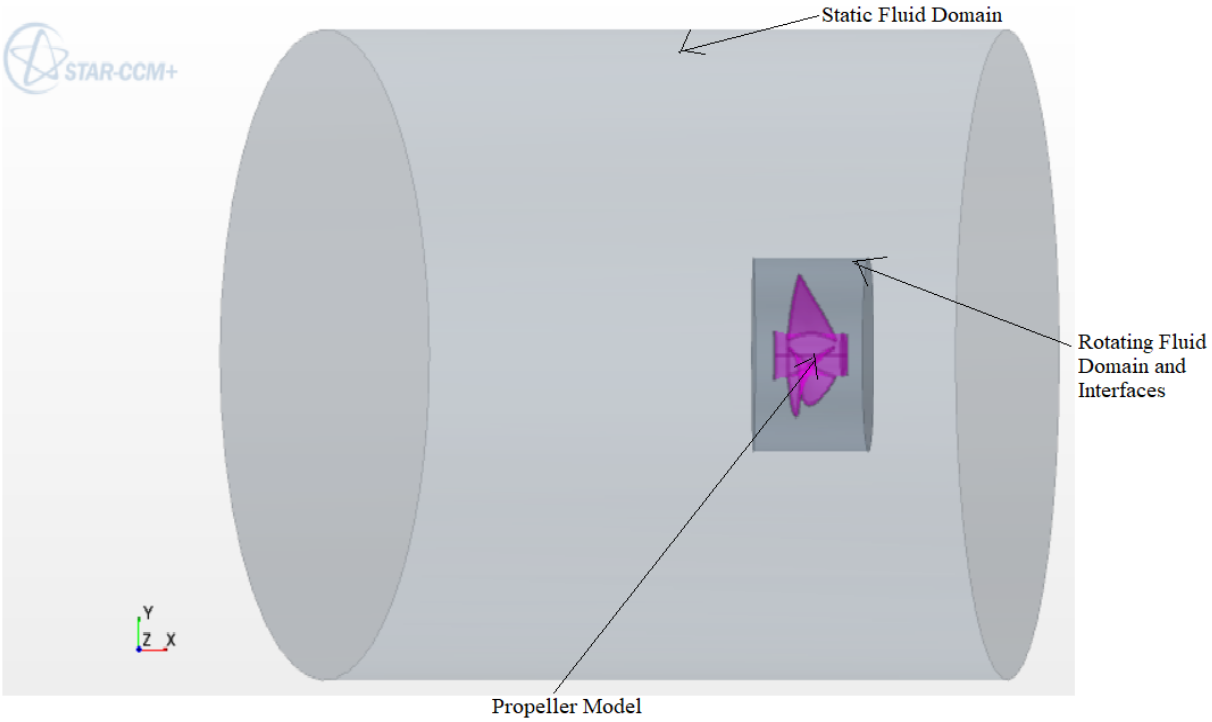

Figure 3.3: Computational Domain within STAR-CCM+

The main dimensions of the computational domain were measured based on the propeller diameter as shown in Figure 3.4. The rotating domain was 1.2D in diameter and 0.5D in length and the static domain of 6D in diameter and 7.5D in length. In the axial direction, the distance of the propeller centre from the inlet and outlet of the computational domain was 2.25D and 5.25D respectively. Naturally, due to shear forces between the fluid layers, it resulted in reversed flow in the "border zone" between the slipstream and the outer domain. When the reversed flow was detected at the domain Outlet, the solver returned a default warning message, since such reversed fluxes were against the very concept of the "pressure outlet" boundary condition. This was one reason why the Outlet boundary was placed so far away from propeller. For steady simulation, the propeller rotation motion was imposed on a rotating region around the propeller by means of rotating reference frame motion. The rest of the domain was set to be stationary as the fixed motion was applied.

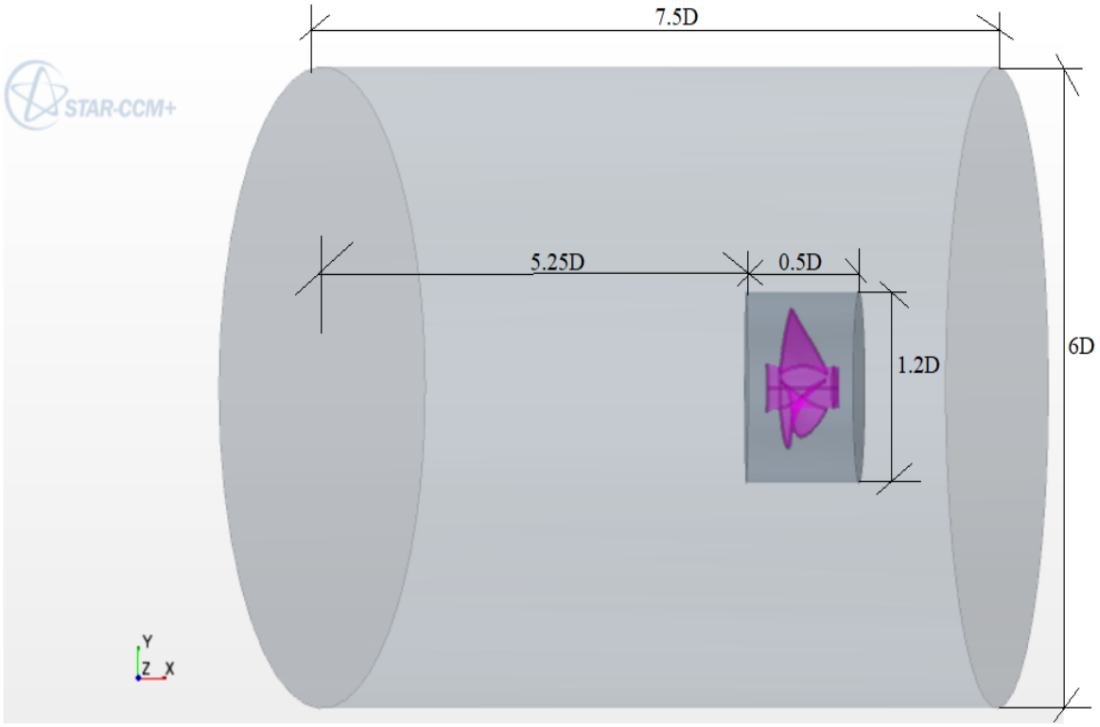

Figure 3.4: Computational Domain Dimensions within STAR-CCM+

3.3.2 Mesh Generation

Mesh generation is a discrete geometrical representation of computational water domain by dividing it into finite cells. Meshing begun by selecting the domain boundaries (surfaces) which enclosed the computational water domain. A volume mesh was built from the surface mesh consisting of three-dimensional elements called cells. The density of faces on a domain boundary (i.e. the size of every face and the distributions) depended on the boundary type, and affected the CFD results. There are different kinds of cell types to be selected from modern CFD codes, such as tetrahedral, hexahedral, pyramid, prism/wedge (Trimmer) and polyhedral. Trimmer mesh was selected for this work due to its accurate results compared to other (Califano & Steen, 2011; Omweri et al., 2017). The required computational efforts such as time for mesh generation, memory and time consumption during numerical solution were compared for the different cells. Complexity of numerical solution algorithm and convergence speed when using trimmer meshes were significantly lesser than the other cells during simulation.

3.3.3 Mesh Model Selection

STAR-CCM+ provides several meshing strategies that are suitable for different applications such as structured and unstructured strategies for generating volume mesh. Due to complexity of the outboard propeller geometry, it was difficult to generate structured mesh. Therefore, unstructured strategy was used. This strategy has different mesh

models including trimmer, polyhedral and tetrahedral in STAR-CCM+ as shown in Appendix B.

According to CD-Adapco (CD-Adapco, 2016) the trimmed and polyhedral cell type meshes produces more accurate solutions when compared to a tetrahedral mesh. Trimmer and polyhedral were compared in this simulation and the results are discussed in Section 4.2.1. In contrast with the polyhedral and tetrahedral models, the trimmer model was not directly dependent on the surface quality of the starting surface and as such was more likely to produce a good quality mesh for most situation. In order to improve the overall quality of an existing surface and optimize it for the volume mesh models, two different kinds of mesh models were selected, that is surface remesher and prism layer mesher. The surface remesher was used to repair the incomplete boundary intersection and creation of periodic interfaces, or to re-triangulate the surface. Surface remeshing on the blade was entirely guided by the values of minimum surface size and target size set up for blade, edges and tip boundaries as shown in Table 3.2. Both target size and minimum size for the blade surface were set up to the same desired value and surface remesher used to do mesh refinement along the blade edges as shown in Table 3.3. Figure 3.5 shows typical mesh generated for outboard propeller using trimmer meshes model. To refine sharp corners and edges of the propeller geometry, and to improve the resolution of flow features, volumetric refinements were applied to the mesh.

This was accomplished by application of volumetric controls (two cylinders and cones) as shown in Figure 3.5 (a) where isotropic refinement method was adopted. Since minor surface flows might still occur at the intersection of the blade with periodic boundaries, the prism layer mesher was used to better resolve flow features near the surface and maintain the first cell height of the solid surface to acceptable margin. This was done in terms of Y^+ factor which is a local Reynolds number ranging from 30 to 500. This Y^+ factor was used to indicate the near-wall treatment characteristic. The mesher projected the core mesh back to the wall boundaries to create prismatic cells. In this study, base size of meshes (9 mm, 15 mm and 20 mm) were also tested to investigate its influence on propeller performance. Since the mesh quality is the main factor for results precision, the finest meshes provide the accurate results as shown in the table3.4. Therefore, the lowest base size was used for all simulations.

Table 3.2: General Mesh Reference Values

Properties		Values	Unit
Base Size		0.009	m
Automatic surface repair	Minimum proximity	0.05	_
	Minimum quality	0.01	_
Number of prism layers		4	_
Prism layer stretching		1.5	_
Prism layer thickness		0.001445	_
Surface size	Relative minimum size	0.5	Percentage of base
	Relative target size	100	Percentage of base

Table 3.3: Boundaries Mesh Customize Setup

Boundaries		Customize surface size	Customize prism mesh	Relative minimum size (% of base)	Relative target size (% of base)
Rotating Region	Blades	Activated	Use default values	4.0	7.5
	Edges	Activated	Use default values	4.0	7.5
	Hub	Activated	Use default values	5.0	15.0
	Interfaces	Not activated	specify custom value	40.0	40.0
Static Region	Inlet	Activated	Use default values	25.0	800.0
	Outlet	Activated	Use default values	25.0	800.0
	Farfield	Activated	Use default values	25.0	800.0
	Interfaces	Not activated	specify custom value	40.0	40.0

Table 3.4: Different Mesh Results for Three Mesh Sizes

Base Size of mesh [m]		0.009	0.015	0.02
Volume mesh representations	Cells	3505042	1268403	725095
	Interior faces	9694355	3530619	2011087
	Vertices	633752	210862	130888

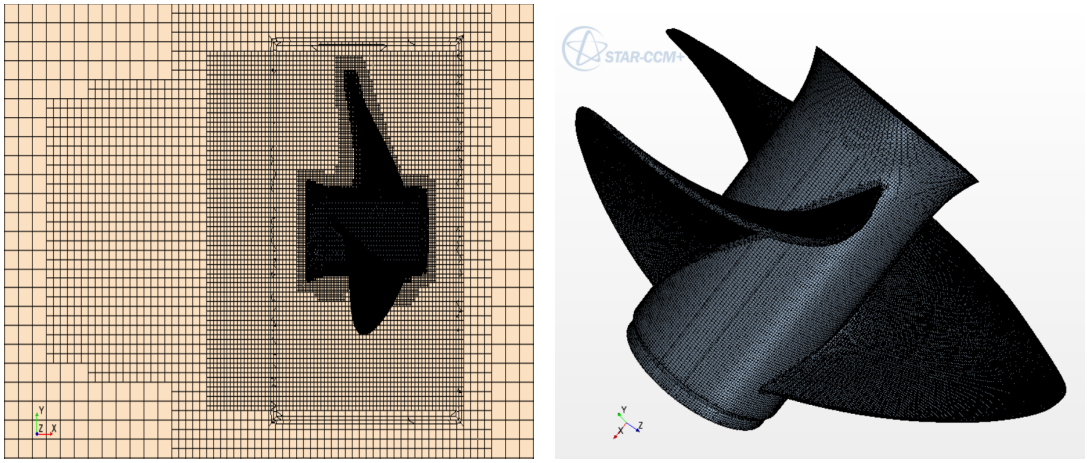

(a) **(b)**

Figure 3.5: Mesh Generated for the RANS Solver (a) Meshes Along the Domain Parts and (b) View of Propeller Model Meshes

3.4 Simulation Study

A geometrical parametric analysis was applied for a different range of number of blades, pitch-to-diameter ratio and rotational speed. The analysis was done for the number of blades between 3-5, within a range of one blade as studied in Ekinci et al.(Ekinci, 2010) experiment. This was to investigate the underlying open water propeller performance characteristics in the experiment on a conventional DTMB4148-propeller. The parameters were simulated to investigate the effect of blade number on propeller performance. The optimum propeller is recommended to be in the range of two to six blades to reduce the resonance as highlighted by John (John, 2012). The efficiency decreased as number of blades increased from three to five which is associated with the high resonance at high advance coefficient.

A range of rotational speed were also simulated to study the effect of rotational speed on propeller performance. The rotational speed of propeller can highly influence performance of the outboard engine. A rotational speed ranging (900-2100 rpm) with an interval of 300 rpm was studied to characterize propeller performance. This range was simalar to what was used by Mashud et al. (Mashud, 2002).

The effects of pitch-to-diameter ratio on propeller performance were also investigated. The pitch effectively converts torque of the propeller shaft to thrust by deflecting or accelerating the water behind as stated by Newton's Second Law of motion (Carlton John, 2012). The pitch-to-diameter ratio was simulated ranging (0.6-1.6) with an interval of 0.2 because the ratio of pitch to diameter, usually falls between 0.5 and 2.5 with an optimal value for most vessels closer to 0.6 to 1.8 (MAN Diesel & Turbo, 2011). This was to evaluate the effects of pitch-to-diameter on open water propeller performance while rotational speed and number of blades were kept constant as studied in Gawn series (M.Faltinsen, 2006) experiment.

3.5 Flow Simulation

3.5.1 Flow Governing Equations

The dynamics of fluid flow is represented by the fundamental laws of physics stating the continuity equation or conservation of mass, momentum, and energy. It is important to note that energy equation is not considered in the marine computational fluid dynamic since the water temperature was taken to be constant.
In this study, a numerical solution for Reynolds-Averaged Navier-Stokes (RANS) Equation was used for solving fluid flow motion using CFD code, STAR-CCM+. This code uses finite volume method to solve the transport equations (Continuity and momentum) (Salvatore et al., 2011). RANS was obtained by applying Reynolds time-averaging to the incompressible form of the navier-Stokes equations to describe the time variation of mean flow quantities. The equations 3.4, 3.9 and 3.13 present the continuity, momentum and RANS equations respectively. Therefore, the general equation of the three-dimensional incompressible (RANS) Equation was used to simulate the performance of the outboard marine propeller(Nath, 2012; Kajishima & Taira, 2017).

1. **Continuity equation:** is a scalar equation reflecting the conservation of mass for a moving fluid. This was expressed in the form shown in Equation 3.3.

$$\frac{\partial \rho}{\partial t} + \frac{\partial (\rho u)}{\partial x} + \frac{\partial (\rho v)}{\partial y} + \frac{\partial (\rho w)}{\partial z} = 0 \tag{3.3}$$

   For the majority of applications in the marine CFD simulation, when the incompressible isothermal flow is applied, the continuity equation becomes;

$$\frac{\partial (u)}{\partial x} + \frac{\partial (v)}{\partial y} + \frac{\partial (w)}{\partial z} = 0 \tag{3.4}$$

where ρ is the fluid density and u, v and w are the flow velocity in X, Y and Z-direction, respectively.

2. **Momentum Equation:** According to the Newton's second law of motion, the momentum equation of the moving fluid element in x, y, and z-direction was expressed as shown in Equations 3.5 to 3.7;

   - X-direction:

$$\rho\frac{Du}{Dt} = -\frac{\partial p}{\partial x} + \frac{\partial \tau_{xx}}{\partial x} + \frac{\partial \tau_{yx}}{\partial y} + \frac{\partial \tau_{zx}}{\partial z} + \rho f_x \tag{3.5}$$

   - Y-direction:

$$\rho\frac{Dv}{Dt} = -\frac{\partial p}{\partial y} + \frac{\partial \tau_{xy}}{\partial x} + \frac{\partial \tau_{yy}}{\partial y} + \frac{\partial \tau_{zy}}{\partial z} + \rho f_y \tag{3.6}$$

   - Z-direction:

$$\rho\frac{Dw}{Dt} = -\frac{\partial p}{\partial z} + \frac{\partial \tau_{xz}}{\partial x} + \frac{\partial \tau_{yz}}{\partial y} + \frac{\partial \tau_{zz}}{\partial z} + \rho f_z \tag{3.7}$$

   Relating the viscous stress in the momentum equation to the rate of linear deformations of the fluid element, the isotropic Newtonian fluids was expressed through the velocity components as follows;

$$\tau_{xx} = 2\mu\frac{\partial u}{\partial x} - \frac{2}{3}\mu\nabla\mathbf{u}, \tau_{yy} = 2\mu\frac{\partial v}{\partial y} - \frac{2}{3}\mu\nabla\mathbf{u}, and\ \tau_{zz} = 2\mu\frac{\partial w}{\partial z} - \frac{2}{3}\mu\nabla\mathbf{u};$$
$$\tau_{xy} = \tau_{yx} = \mu\left[\frac{\partial v}{\partial x} + \frac{\partial u}{\partial y}\right], \tau_{xz} = \tau_{zx} = \mu\left[\frac{\partial u}{\partial z} + \frac{\partial w}{\partial x}\right], \tau_{yz} = \tau_{zy} = \mu\left[\frac{\partial w}{\partial y} + \frac{\partial v}{\partial z}\right] \tag{3.8}$$

   Substituting Equation 3.8 into Equations of the momentum equations in X, Y, and Z directions. The equations appeared in the form Equations 3.9 to 3.11;

   - X-direction:

$$\rho\frac{Du}{Dt} = -\frac{\partial p}{\partial x} + \frac{\partial}{\partial x}\mu\left(2\frac{\partial u}{\partial x} - \frac{2}{3}\nabla\mathbf{u}\right) + \frac{\partial}{\partial y}\left[\mu\left(\frac{\partial v}{\partial x} + \frac{\partial u}{\partial y}\right)\right] + \frac{\partial}{\partial z}\left[\mu\left(\frac{\partial u}{\partial z} + \frac{\partial w}{\partial x}\right)\right] + \rho f_x \tag{3.9}$$

- Y-direction:

$$\rho\frac{Dv}{Dt} = -\frac{\partial p}{\partial y} + \frac{\partial}{\partial x}\left[\mu\left(\frac{\partial v}{\partial x} + \frac{\partial u}{\partial y}\right)\right] + \frac{\partial}{\partial y}\mu\left(2\frac{\partial v}{\partial y} - \frac{2}{3}\nabla\mathbf{u}\right) + \frac{\partial}{\partial z}\left[\mu\left(\frac{\partial u}{\partial z} + \frac{\partial w}{\partial x}\right)\right] + \rho f_y \tag{3.10}$$

- Z-direction:

$$\rho\frac{Dw}{Dt} = -\frac{\partial p}{\partial z} + \frac{\partial}{\partial x}\left[\mu\left(\frac{\partial u}{\partial z} + \frac{\partial w}{\partial x}\right)\right] + \frac{\partial}{\partial y}\left[\mu\left(\frac{\partial w}{\partial y} + \frac{\partial v}{\partial z}\right)\right] + \frac{\partial}{\partial z}\mu\left(2\frac{\partial w}{\partial z} - \frac{2}{3}\nabla\mathbf{u}\right) + \rho f_z \tag{3.11}$$

In the honor of the two men namely the Frenchman M. Navier and Englishman G.Stokes in 19^{th} century, the above scalar equations were obtained and so called Navier-Stokes Equations (Kajishima & Taira, 2017).
where, $\frac{D}{Dt} = \frac{\partial}{\partial t} + u\frac{\partial}{\partial x} + v\frac{\partial}{\partial y} + w\frac{\partial}{\partial z}$ is the substantial derivative, $\nabla\mathbf{u} = \frac{\partial u}{\partial x} + \frac{\partial v}{\partial y} + \frac{\partial w}{\partial z}$ is the convective derivative, μ is the dynamic viscosity, p is the static pressure, $f_x, f_y and\ f_z$ are the mass forces and ρ is the fluid density.

3. **Reynolds-Averaged Navier-Stokes (RANS) Equation**

In this work, the flow governing equation was provided by Reynolds-Average-Navier Stokes (RANS) Equations. Applying Reynolds time-averaging to the incompressible form of the navier-stokes equations given in the Equation 3.9 led to the Reynolds Averaged Navier-Stokes (RANS) equations 3.13 describing the time variation of mean flow quantities. The assumption made to simplified the navier stokes equations are that;

1. Temperature and energy are usually not taken account. This means that for marine problem, energy conservation equation is not used.
2. Flow is incompressible and steady
3. Viscosity is constant
4. Fluid flows are turbulent
5. The components of flow velocity and pressure are represented of their mean values and turbulent fluctuations as shown in the Equation 3.12.

$$U = \bar{u} + u',\ V = \bar{v} + v',\ W = \bar{w} + w',\ and\ P = \bar{p} + p' \tag{3.12}$$

where; $U, V, and\, W$ are the momentary velocity components,$\bar{u}, \bar{v}, and\, \bar{w}$ are the velocity time-averaged value or mean value and $u', v', and\, w'$ are the fluctuating velocities. The time-averaged values of the fluctuating values were defined to be variables and the mean value of the velocities were taken as constant. Hence, the Equations 3.9 to 3.11 become;

- x-components:

$$\rho\left[\frac{\partial \bar{u}}{\partial t} + \bar{u}\frac{\partial \bar{u}}{\partial x} + \bar{v}\frac{\partial \bar{u}}{\partial y} + \bar{w}\frac{\partial \bar{u}}{\partial z}\right] = -\frac{\partial p}{\partial x} + \mu\frac{\partial^2 \bar{u}}{\partial x^2} + \mu\frac{\partial^2 \bar{u}}{\partial y^2} + \mu\frac{\partial^2 \bar{u}}{\partial z^2} - \frac{\partial}{\partial x}\left(\rho\overline{u'u'} + \rho\overline{u'v'} + \rho\overline{u'w'}\right) \tag{3.13}$$

- y-components:

$$\rho\left[\frac{\partial \bar{v}}{\partial t} + \bar{u}\frac{\partial \bar{v}}{\partial x} + \bar{v}\frac{\partial \bar{v}}{\partial y} + \bar{w}\frac{\partial \bar{v}}{\partial z}\right] = -\frac{\partial p}{\partial x} + \mu\frac{\partial^2 \bar{v}}{\partial x^2} + \mu\frac{\partial^2 \bar{v}}{\partial y^2} + \mu\frac{\partial^2 \bar{v}}{\partial z^2} - \frac{\partial}{\partial x}\left(\rho\overline{v'u'} + \rho\overline{v'v'} + \rho\overline{v'w'}\right) \tag{3.14}$$

- z-components:

$$\rho\left[\frac{\partial \bar{w}}{\partial t} + \bar{u}\frac{\partial \bar{w}}{\partial x} + \bar{v}\frac{\partial \bar{w}}{\partial y} + \bar{w}\frac{\partial \bar{w}}{\partial z}\right] = -\frac{\partial p}{\partial x} + \mu\frac{\partial^2 \bar{w}}{\partial x^2} + \mu\frac{\partial^2 \bar{w}}{\partial y^2} + \mu\frac{\partial^2 \bar{w}}{\partial z^2} - \frac{\partial}{\partial x}\left(\rho\overline{w'u'} + \rho\overline{w'v'} + \rho\overline{w'w'}\right) \tag{3.15}$$

where; $\rho\bar{u'}\bar{u'}$, $\rho\bar{u'}\bar{v'}, and\ \rho\bar{u'}\bar{w'}$ etc.. are Reynolds stresses that arise from the turbulent nature of the flow. Different methods can be chosen in CFD program to solve the governing equations. Among them are, discretization methods such as finite difference, finite element and finite volume methods. These methods use turbulence model like algorithm pressure based solvers (segregated or coupled algorithm) in their solution procedure. In this work, finite volume methods and segregated flow solver were used. Finite volume methods is a discretization methods used for the approximation of the surface and volume integrals that represent different terms of the equations governing transport of solution variables. Numerically, this approximation allows to convert a general scalar transport equation to an algebraic equation that can be solved at one time. The segregated flow solver was used to control the velocity and pressure solver.

The pressure solver solved the discrete equation for pressure correction to update the pressure field while the velocity solver solved the discrete momentum equation to obtain the velocity field.

3.5.2 Boundary Conditions

In the beginning of simulation, the solution was prepared for the entire computation domain. Computation domain was also restricted to different types of boundaries such as inlet, outlet, far field, and interfaces as shown in Figure 3.6. The inlet boundary was treated as a velocity inlet and calculated as shown in Table 3.5, whereas a pressure outlet condition was adopted for the outlet boundary and a symmetry plane condition for the far field.

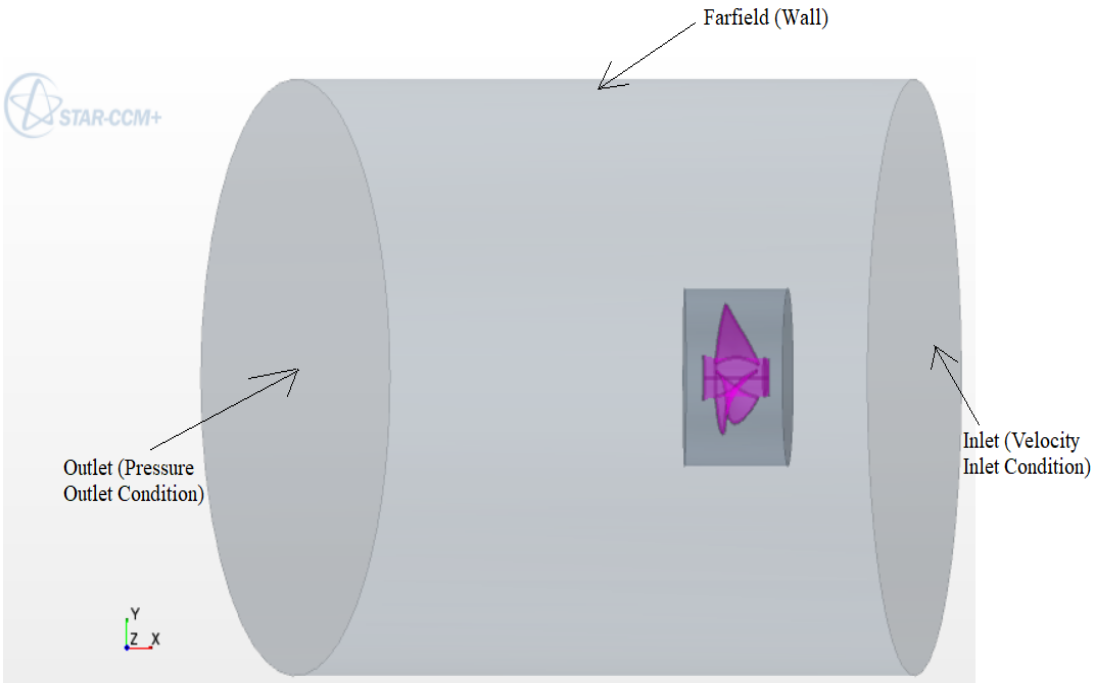

Figure 3.6: Boundaries Condition within Star CCM+9.06

The simulation domain was also initialized by supplying the values of velocity components and turbulence characteristics. It follows that for the flow equations to be solved, each cell has to be initialized by setting up preliminary solution data to the primary variables associated with the model at the time step zero ($t = 0$). For the inlet boundary, the velocity needed to be input into the pre-processor. In the propeller model simulation with an advance ratio (J), the advance velocity of propulsor was computed from Equation 2.5, and the propeller velocity is given as;

$$V_a = NDJ \tag{3.16}$$

where, V_a is the propeller speed advance, N is the rotational speed, D is the propeller diameter, and J is the advance coefficient. In addition for the outlet boundary, the static pressure was set to zero corresponding to the atmospheric pressure. In this work, only the conditions with advance ratio (J= 0.1, 0.3, 0.5, 0.7, 0.9, 1.1, 1.3) were simulated following the trends found on the Open Propeller Performance Characteristics Curves (M.Faltinsen, 2006). The propeller revolution (N) was set to 900 rpm and changed to the desired study. Hence, the velocities of propeller under different advance ratio are summarized in the Table 3.5.

Table 3.5:]
Propeller Velocity Component in [m/s]

Advance ratios (J)	**0.1**	**0.3**	**0.5**	**0.7**	**0.9**	**1.1**	**1.3**
Propeller velocities (V_a)	0.455	1.364	2.273	3.182	4.091	5.0	5.91

3.5.3 Physical Models Selection

The following physical models were selected to investigate the fluid flow field and open water propeller performance of the outboard propeller:
Three dimensional → Steady → Liquid → segregated flow → Constant density → Turbulent → K-ω turbulence → Gradients → Turbulence Suppression → Cell quality-Remediation → All Y^+ wall treatment. All these were selected as shown in Table 3.6. In the Table 3.6, the Reynolds-Averaged Navier-Stokes (RANS) was selected.

Table 3.6: Physical Models Selection in STAR-CCM+

Selected Models
Three Dimensional
Steady flow
Liquid (Water)
Constant density (998.67 Kg/m^3)
Constant viscosity(0.001068 Pa-s)
Turbulent flow
Reynolds-Averaged-Navier-Stokes (RANS)
K-ω turbulence
SST(Menter) K-ω
Segregate flow algorithm
All Y^+ wall treatment
Gradients
Turbulence Suppression
Cell quality-Remediation

The turbulence phenomena was captured when selecting the turbulent flow. Turbulent

flow is the flow in which separate layers of fluid flow are mixed. It is characterized by the local Reynolds number greater than 4000. It is also called the chaotic vertical flow. In this study, in order to simplify the equations, the fluid was assumed to be at 100% turbulent flow. This resulted in the presentation of the components of the flow velocity as a superposition of their mean values and turbulent fluctuations. The Reynolds number is determined by the Equation in Appendix A.8 derived by Techet et al. (A.H.Techet, 2004).

$$R_n = \frac{\rho N D^2}{\mu} \tag{3.17}$$

The All Y^+ wall treatment was selected to solve the near-wall problem because it contains both high and low y^+conditions. Y^+ is similar to the local Reynolds number.

$$Y^+ = \frac{y.U_t}{\nu} \tag{3.18}$$

where, U_t is the friction velocity, ν is the kinematic viscosity and y is the distance between the cell centroid and wall boundary. For the normal simulation, the y^+ number should be in range 30-500 so that can keep the result accurate (CD-Adapco, 2016).

In STAR-CCM+, the primary function of the space models is to provide methods for computing and accessing mesh metrics. Due to the relevance of the spatial directions in this work, the three-dimensional model was selected to work on three-dimensional meshes. To control the iteration stepping, the steady model was used for all steady-state calculations. This means that only spatial derivatives are discretized. In steady state calculations, the arbitrary states are integrated to the asymptotic solution in any manner to get a least amount of computational work. The fluid flow properties like density, viscosity were defined as constant for this simulation. In CFD, since the governing equation are non-linear and coupled, the solution loop must be carried out iteratively in order to obtain a converged numerical solution. The segregated flow was chosen in this study as a solution algorithm to solve the governing equations sequentially because it has ability to handle one equation at one time. In the segregated algorithm, the individual governing equations for the solution variables are solved step by step. Each governing equation, while being solved, is "decoupled" or "segregated" from other equations, hence its name. The segregated algorithm saved the computer memory, since the discretized equations need only be stored in the memory one at a time. However, the solution convergence was relatively slow, in as much as the equations were solved in a decoupled manner.

3.5.4 Turbulent Models

In this study, in order to simplify the equations, the fluid was assumed to be at 100% turbulent flow. The turbulence phenomena was captured when selecting the SST (Shear Stress Transport) k-ω turbulence model for turbulence closure. The turbulent closure were modeled by turbulence model, semi-empirical using experimental and statistical data. The RANS method resolved only the vortices of the largest scale comparable with the size of flow domain. There was a closure problem in the RANS equation because of the non-linear term Reynolds stress. The turbulent dynamic viscosity coefficient (μ_t) was therefore introduced into the RANS equation to close equation as shown in the user-guidance of STAR-CCM+ (CD-Adapco, 2016). The turbulence model is required to be constructed based on the required number of differential equation determined by μ_t. The turbulence models are usually built by the zero-equation model, one-equation model (Spalart-Allmaras model) and two-equation model (k-ε , k-ω model) (Menter, 1994). K-ε and k-ω models were tried in this study and the results obtained using k-ω models were accurate and convergent compared to k-ε models.

The SST (Shear Stress Transport) k-ω turbulence model was chosen for turbulence closure. It was also selected to deal with the strong free stream sensitivity of the k-ω turbulence model. The k-ω turbulence models represent a group of two-equation turbulence models in which the transport equation were solved for the turbulent kinetic energy (k) and its specific dissipation rate (ω) as shown in the Equation 3.19 and 3.21, respectively.

It is currently one of the most widely used turbulence models for a marine machinery applications. The advantages of this model were seen in its ability to handle simultaneously lower-Reynolds number and higher-Reynolds number zones in the flow, and to predict more accurately non-equilibrium regions in the boundary layer with adverse pressure gradients such as observed when separation occurs. The above considerations were important when modeling full and model scale propellers operating at heavy loading(CD-Adapco, 2016; Menter, 1994).

- Turbulence Kinetic Energy (k):

$$\frac{\partial k}{\partial t} + U_j \frac{\partial k}{\partial x_j} = \tau_{ij} \frac{\partial u_i}{\partial x_j} - \beta^* k\omega + \frac{\partial}{\partial x_j}[(\upsilon + \sigma^* \frac{k}{\omega}) \frac{\partial k}{\partial x_j}] \tag{3.19}$$

- Specific Dissipation rate (ω):

$$\frac{\partial \omega}{\partial t} + U_j \frac{\partial \omega}{\partial x_j} = \alpha \frac{\omega}{k} \tau_{ij} \frac{\partial u_i}{\partial x_j} - \beta \omega^2 + \frac{\sigma_d}{\omega} \frac{\partial k}{\partial x_j} \frac{\partial \omega}{\partial x_j} + \frac{\partial}{\partial x_j}[(\upsilon + \sigma \frac{k}{\omega}) \frac{\partial \omega}{\partial x_j}] \quad (3.20)$$

- Turbulent Eddy viscosity (υ_t):

$$\upsilon_t = \frac{k}{\bar{\omega}} \quad (3.21)$$

where,
$\bar{\omega} = max[\omega, C_{lim} \frac{\frac{\partial u}{\partial y}}{\sqrt{\beta^*}}]$
$\alpha = \frac{13}{25}$, $\beta^* = \frac{9}{100}$, $\sigma = \frac{1}{2}$, $\sigma^* = \frac{3}{5}$.

3.6 Open Water Propeller Performance Characteristics

The main variable under investigation within STAR-CCM+ was the change in propeller performance which depends on the thrust, torque, and efficiency. These were set up and determined by non-dimensional quantities through propeller performance, which are, thrust coefficient(K_T), torque coefficient (K_Q), and open propeller efficiency(η_o) and plotted with respect to the advance coefficient (J). The expressions for K_T,K_Q, η_o and J are given in Equations 3.22 to 3.25 as shown in (A.H.Techet, 2004) and its derivation is also shown in Appendix A.

- Thrust coefficient (K_T):

$$K_T = \frac{T}{\rho N^2 D^4} \quad (3.22)$$

- Torque coefficient (K_Q):

$$K_Q = \frac{Q}{\rho N^2 D^5} \quad (3.23)$$

- Advance coefficient (J):

$$J = \frac{V_a}{ND} \quad (3.24)$$

- Open water efficiency (η_0):

$$\eta_o = \frac{K_T}{K_Q} . \frac{J}{2\pi} \quad (3.25)$$

where, T is the thrust, Q is the torque, D is the diameter, N is the rate of rotation, ρ is the density of the fluid, g is the acceleration due to gravitation and V_a is advanced Speed of rotating body or propeller speed.

The advance coefficients (J) ranging from 0.1 to 1.3 were used to study the propeller performance and the propeller revolution was set up to 900 rpm and then changed when studying the rotational speed effect. According to the moving reference frame the simulation was performed for the steady-state case only. Numerical methods STAR-CCM+ employs Moving Reference Frame (MRF) approach to perform simulation on a rotating body. This method involves manipulating the equations of motion into the rotating frame in different ways. MRF method involves rewriting the time-averaged, steady-state form of the Navier-Stokes equations in a moving frame. Moreover, the MRF is therefore an excellent approach to the prediction of propeller open water characteristics and also its flexibility and low CPU demand made it widespread use in the marine and turbo-machinery industry. In numerical flow setup, the propeller thrust (T) was examined as a drag force on the propeller blades by integrating pressure and viscous shear over the blades and hub surfaces while the propeller torque (Q) was monitored as a moment resulting from pressure and viscous shear force over the blades and hub surfaces.

3.7 Definition and Export of the Output Results

In this study, simulation utilized some basic post-processing instructions in STAR-CCM+. A chart was used to extract the simulated data, which was exported to Microsoft Excel to generate the output data, then exported to OriginPro 9.1 for plotting of graphs for analysis. In cases where the solution failed to converge, the finite volume mesh and the analysis iteration setup were modified, and the simulations were repeated. Figure 3.7 shows a flowchart summarizing the simulation procedure.

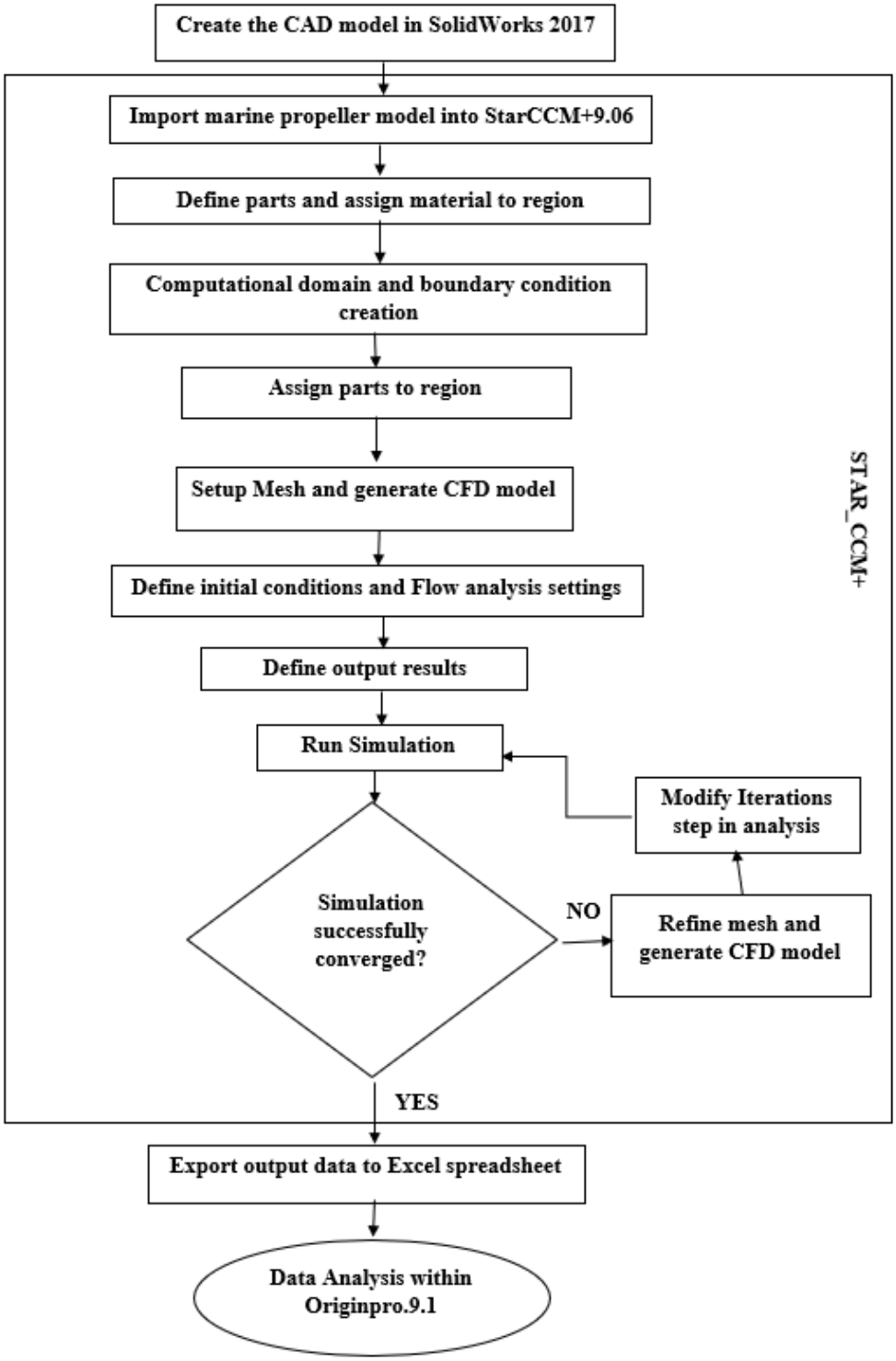

Figure 3.7: Flowchart for Propeller Performance Analysis in STAR-CCM+

3.8 Convergence Study

The convergence of the results was determined using two different approaches which are the behavior of the key parameters (Torque and Thrust coefficient and open pro-

peller efficiency) and the trend of residuals (CD-Adapco, 2016). Figures 3.8 (a) and (b) show the convergence for steady simulations controlled by residuals and the values of torque coefficient (K_Q) and thrust coefficient (K_T) for the iteration step up to 3000. The values illustrated on the residual curves were the solution of the RANS equations and turbulence models equations. Shown in Figure 3.8(a) is the plots for convergence of 6 values: one continuity equation; three momentum convergence equations in X, Y, Z directions; Tke and Sdr equations (for SST k-ω) as well as propeller performance characteristics of torque and thrust coefficients. In Figure 3.8 (a), the large oscillations were observed during the first iterations up to 1800 iterations, after which the results became stable and converged to the final solution with small variations. Convergence occurred when the residuals curves crossed the error at 0.1 as seen in Figure 3.8. It is noted that in Figure 3.8 (a) that three momentum convergence equations in X, Y, Z components stabilizes initially after 1400 iterations, one continuity and Tke equations stabilizes initially after 1200 iterations and Sdr equation stabilizes after 1000 iterations. In Figure 3.8(b) both torque and thrust coefficients stabilizes before 1000 iterations and stabilizes after 1600 iterations. The simulations took up to an average of 72 hours for the solution to converge.

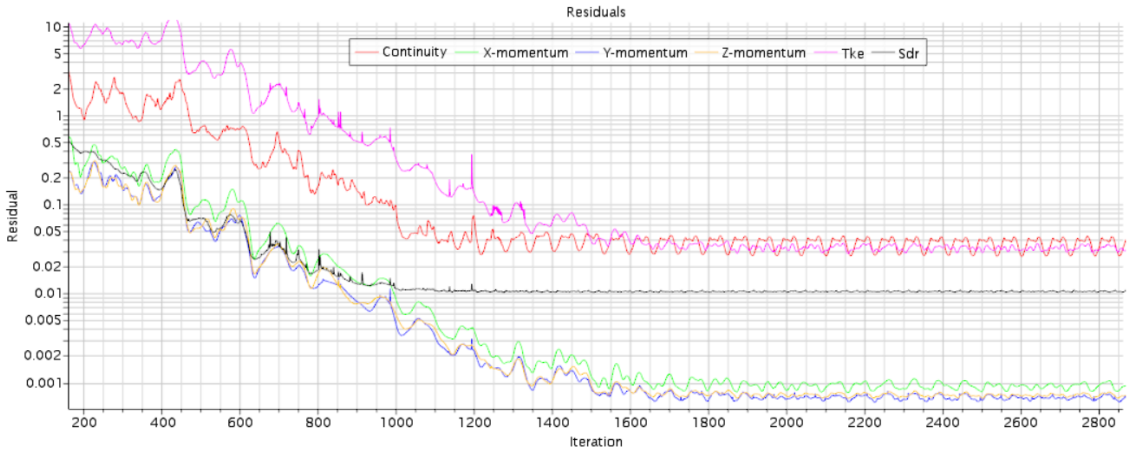

(a) Residuals Plot for Steady Simulation at J=0.1

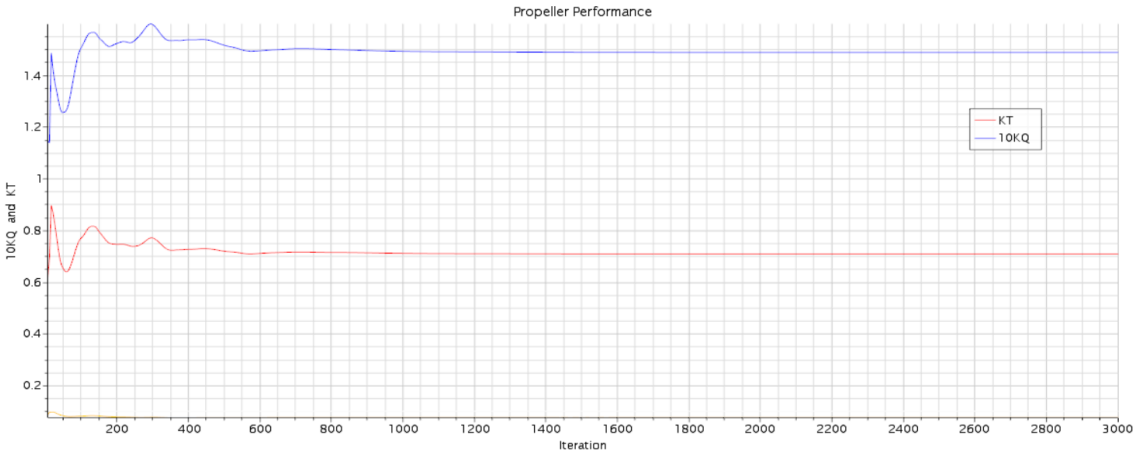

(b) 10KQ, and KT Plot for Steady Simulation at J=0.1

Figure 3.8: Convergence Study for Steady Simulation at J=0.1

CHAPTER FOUR
RESULTS AND DISCUSSION

4.1 Introduction

This chapter presents the results obtained from modeling the behavior of outboard engine propeller using CFD. The influence of blade number, pitch to diameter ratio and rotational speed on propeller performance are also discussed and presented. Simulation results were compared to existing data obtained from literature. The fluid flow fields (velocity and pressure flow field around the propeller blade) were also studied. A mobile workstation with 16 GB RAM, Dual Core - 2.7 GHz CPU and 500 GB HDD and 258 GB SCD was used. Each of the simulations took up to an average of 72 hours for the solution to converge.

4.2 Effect of Meshes on Marine Propeller Performance

The investigated mesh types were trimmer and polyhedral. The effect of base sizes of the trimmer mesh were also studied.

4.2.1 Effect of Types of Meshes

In this section, the comparison of the results for the trimmer (prismatic) mesh and a polyhedral mesh with respect to open water propeller performance is presented. The Figure 4.1 shows results of open water propeller performance based on trimmer and polyhedral mesh types. In Figure 4.1 (a) and 4.1 (b), the highest thrust and torque coefficient of 17.6% and 4.7% respectively were observed at the lowest advance coefficient (J) of 0.1 and reduced to 1.8 % and 0.18% respectively at high advance coefficient (J) of 1.3 for trimmer mesh. Also the highest thrust and torque coefficient of 7.3% and 1.5% respectively were obtained at the lowest advance coefficient (J) of 0.1 and reduced to -2.4% and 0.017% respectively at high advance coefficient (J) of 1.3 for polyhedral mesh. These was attributed to the required high load for propeller to start (H. Kutty & Rajendran, 2017).

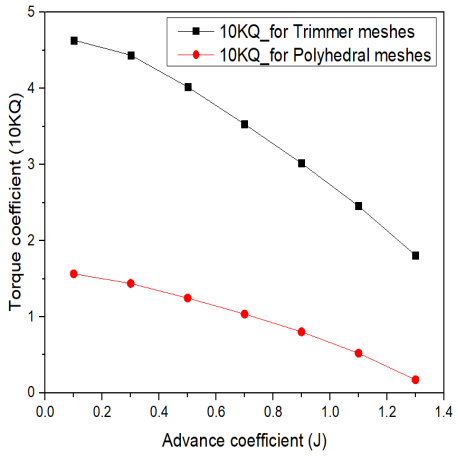

(a) Torque Coefficient

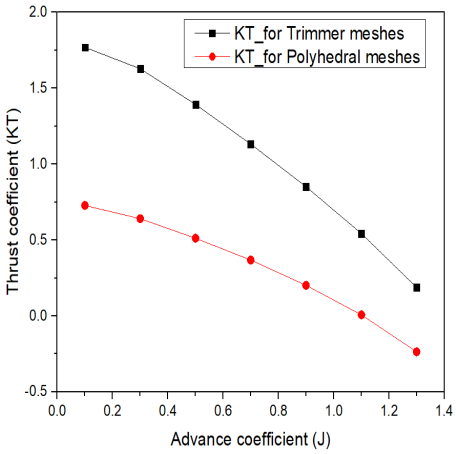

(b) Thrust Coefficient

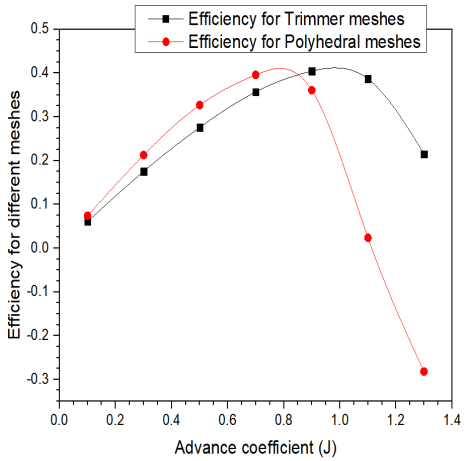

(c) Efficiency

Figure 4.1: Performance Comparison of Mesh Types

In Figure 4.1 (c) each type of mesh had a maximum (peak) efficiency with respect to advance coefficient. It was observed from the Figure 4.1 (c) that in the range of low-speed boats i.e, (J=0.1, 0.3, 0.5, 0.7 and 0.9), the polyhedral meshes had high peak efficiency of 39.6% compared to trimmer meshes. The trimmer mesh had the maximum efficiency of 35.7% at J= 0.7. It was also found that in the range of J=1.1 and 1.3, trimmer mesh had the peak efficiency of 41%. These observations are in agreement with the findings of Hai-long et al. (Hai-Long et al., 2016) who investigated the scale effects for rudder bulb and rudder thrust fin on propulsive efficiency based on computational fluid dynamics and Kutty et al. (H. Kutty & Rajendran, 2017) in the investigation of small scale propeller performance. Therefore, Trimmer mesh was selected to investigate the propeller performance improvement of high-speed boat running on an outboard engine, since it had a better convergence than the polyhedral meshes.

4.2.2 Effect of Base Sizes of Trimmer Mesh

After selecting trimmer mesh, this study investigated the effect of base size of 9 mm, 15 mm and 20 mm to get the proper mesh setups in STAR-CCM+. Figure 4.2 shows the propeller performance characteristic under difference mesh size. In Figure 4.2(a), the highest torque coefficient increased by 0.004% as base sizes increased at the advance coefficient (J) of 0.1. In Figure 4.2(b), the highest thrust coefficient reduced by 0.3% with base size at the advance coefficient (J) of 0.1. It was also observed that the peak efficiency was 69% at base size of 9 mm.

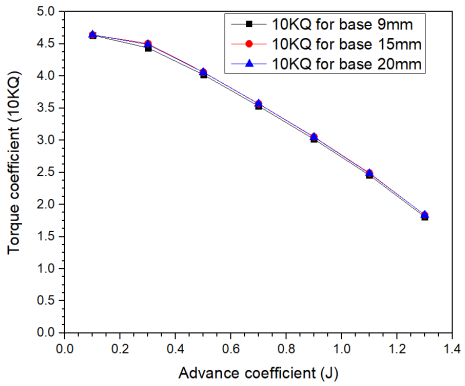

(a) Torque Coefficient ($10K_Q$)

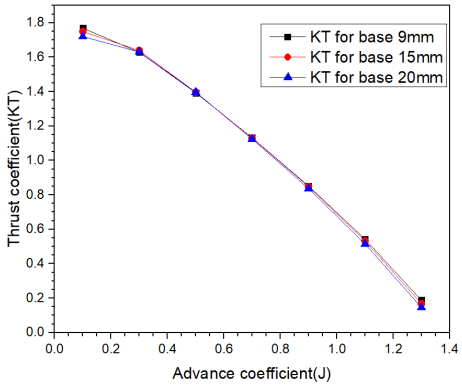

(b) Thrust Coefficient (K_T)

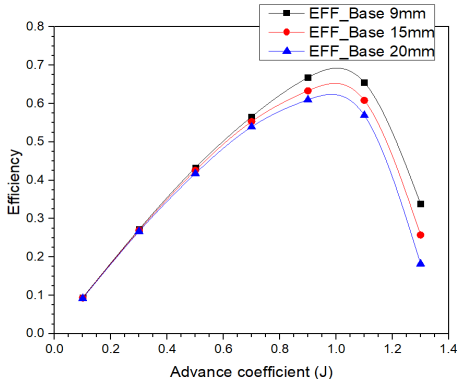

(c) Open water efficiency (η_0)

Figure 4.2: Performance Comparison of Base Sizes for J= 0.1 to 1.3

In Figure 4.2(c), efficiency η_0 decreased by 5.8% with base size at the advance coefficient (J) of 1.1. This was attributed to numerical set up and solver selections. This agreed with the results of numerical simulation of the flow around marine propeller series done by Boucetta et al. (Boucetta & Imine, 2016). The simulation results show little difference on the open water characteristics as shown in Figure 4.2. There is only a marginal difference between the results for a specific advance coefficient (J) as stated above. However, the required time of the simulation for the case with the base size of 9

mm, 15 mm and 20 mm was about 72, 60 and 40 hours, respectively. This observation agrees with the findings of Zhao (Zhao Yaning, 2015) who studied the scale effects on propellers with different magnitude of skew by CFD Methods. Similar agreement was observed in the work of Boucetta et al. (Boucetta & Imine, 2016). It is important to conclude that the fined mesh gives more reliable results compared to the two others. Therefore, the base size of 9 mm was applied to all the simulations.

4.3 Effect of Geometrical Parameters on Marine Propeller Performance

4.3.1 Effect of Number of Blades

The open water characteristics of propellers (thrust coefficient, torque coefficient and efficiency) with different advance coefficients (J= 0.1, 0.3, 0.5, 0.7, 0.9, 1.1, and 1.3) were obtained. Figure 4.3 shows the propeller performance characteristics (thrust coefficient, torque coefficient and efficiency). Using the linear regression from Excel

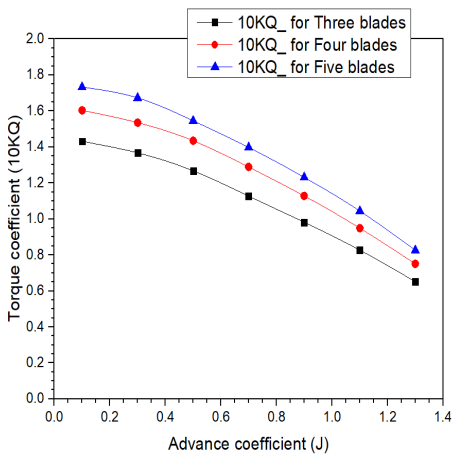

(a) Torque Coefficient

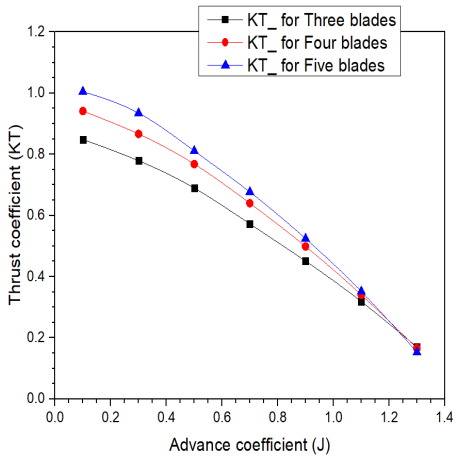

(b) Thrust Coefficient

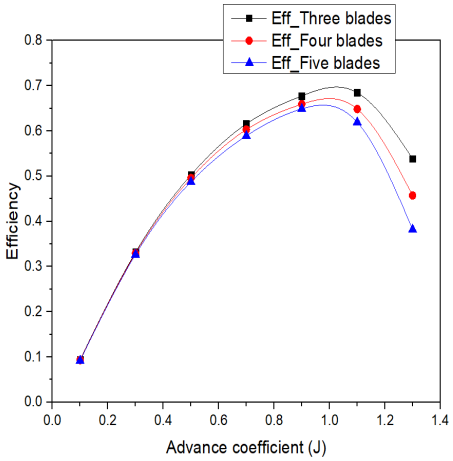

(c) Efficiency

Figure 4.3: Performance Comparison of Blade Numbers for J=0.1 to 1.3

spreadsheet, it was found that the torque coefficient decreased by 76%, 72% and 66% as the number of blades decreased from five to three blades, respectively. This can be attributed to the frictional component and sensitivity of viscous stresses exerted on the propeller blades. Similar agreement was reported in the results of Baquero *et al.* (A. Baquero and A.Haimov, 1999) in experimental validation of marine propeller performance. It was also observed that thrust coefficient decreased by 71%, 65% and 57% for propeller with five, four and three blades, respectively. It is due to propeller parts geometry such as rotational speed and propeller diameter. This agrees with the findings made by Mashud et al. (Mashud, 2002) who investigated the effect of geometrical parameters on open water propeller performance.

Figure 4.3 (c) shows the propeller efficiency behavior with the advance coefficient. The maximum propeller efficiencies of 64.9%, 65.9% and 70.8% were observed for the propeller with five, four and three blades, respectively. This was observed at advance coefficient (J) of 0.9. The results showed that a decrease in blade number increased the propeller efficiency by 6%. This could be attributed to numerical set up and solver selections. This agreed with the experimental data of marine propeller performance presented by Baquero *et al.* (A. Baquero and A.Haimov, 1999) but disagreed with numerical results found by Boucetta et al. (Boucetta & Imine, 2016) while optimizing the marine propeller based on number of blades, skew magnitude, and blade thickness. He found an efficiency of 60% and 58% for the propeller with four and three blades respectively. The discrepancy in results can be attributed to the computational code and polyhedral grids used.

4.3.2 Effect of Rotational Speed

The effects rotational speed on open water performance of propellers were analyzed. The performance characteristics of thrust coefficient and torque coefficient with different rotational speed of 900, 1200, 1500, 1800, and 2100 rpm were presented. Figure 4.4 shows the variation of propeller performance characteristics with varying rotational speed. The minimum torque and thrust coefficient reduction of 66% and 57% respectively were found with rotational speed of 900 rpm as shown in Figure 4.4 (a) and 4.4 (b). This led to high propeller efficiency (71%). This was attributed to the frictional component and sensitivities of viscous stresses exerted on the propeller blades as rotational speed increased. According to Omweri et al. (Omweri et al., 2017), the turbulent transition at the highest load (J from 0.7 to 1.3) results to difficulties in numerical simulation. Mashud et al. (Mashud, 2002) also found that the increase

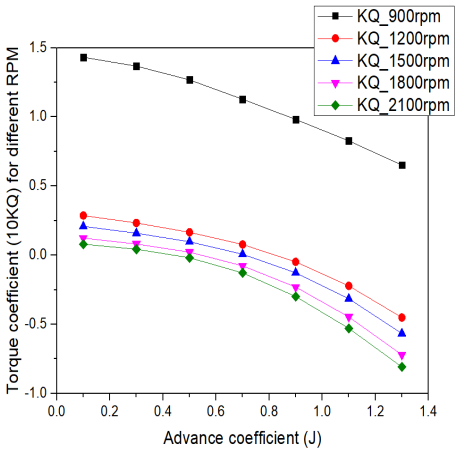

(a) Torque Coefficient

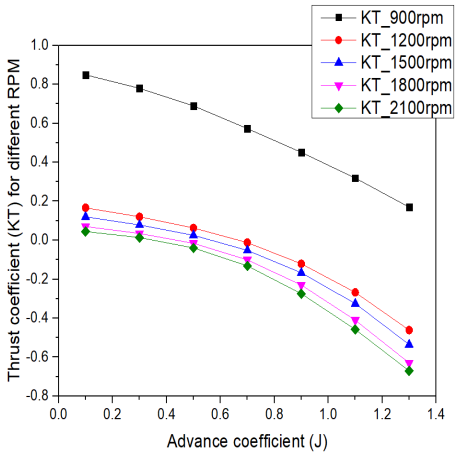

(b) Thrust Coefficient

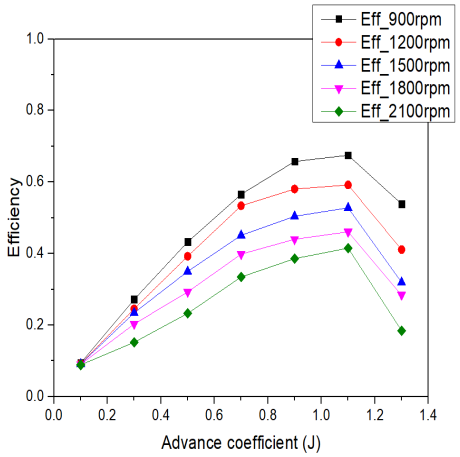

(c) Efficiency

Figure 4.4: Propeller Performance of Various RPM for J= 0.1 to 1.3

in rotational speed increased the horsepower which in turn reduced the propeller performance characteristics. Figure 4.4 (c) shows the propeller efficiency behavior with the advance coefficient. The maximum propeller efficiencies of 71%, 59.2%, 52%, 46% and 39.2% were observed for 900, 1200, 1500, 1800, and 2100 rpm, respectively. This was observed at advance coefficient (J) of 1.1. Using linear regression, the results showed that an increase in rotational speed reduced the propeller efficiency by 8.1%. This could be attributed to the appropriate assumption that the flow around propeller was fully turbulent. This agreed with the experimental data of marine propeller performance presented by Mashud et al.(Mashud, 2002).

4.3.3 Effect of Pitch-to-Diameter Ratio (P/D)

Numerical simulation was performed to study the effect of the pitch-to-diameter ratio (P/D) on the open water performance. Based on results from sections 4.3.1 and 4.3.2,

three-blade propeller was rotated at 900rpm. P/D ratio range from 0.6 to 1.6 for a propeller was studied. Figure 4.5 shows the propeller performance characteristics of thrust coefficient, torque coefficient and efficiency for various pitch-to-diameter ratios.

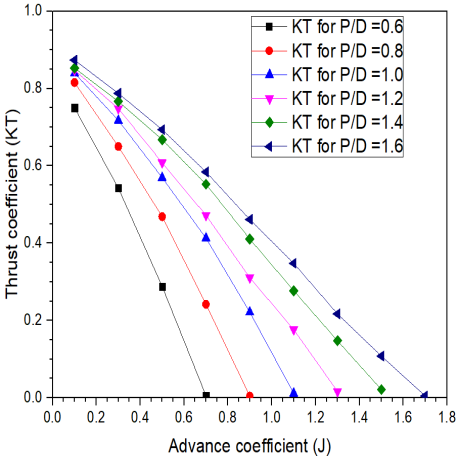

(a) Thrust Coefficient

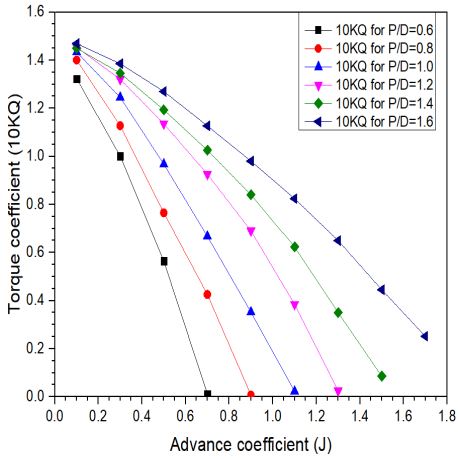

(b) Torque Coefficient

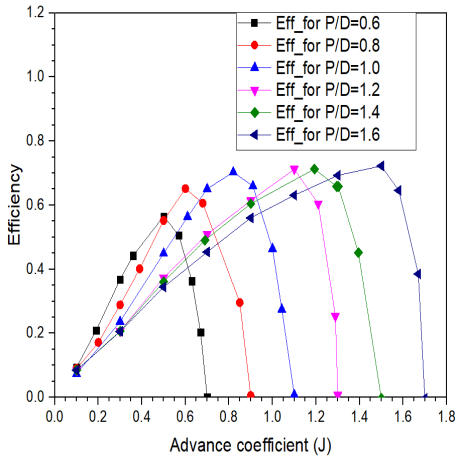

(c) Efficiency

Figure 4.5: Propeller Performance Comparison for Different Values of P/D

In the Figure 4.5 (a), it was found that the thrust coefficient decreased by 94%, 90%, 80.6%, 70%, 60% and 55.8% for propeller with pitch-to diameter ratios of 0.6, 0.8, 1.0, 1.2, 1.4, 1.6 respectively. Figure 4.5 (b) shows the torque coefficient for CFD results. The torque coefficient showed the largest values at P/D= 1.6 for all the advance ratios while the values at P/D = 0.6 represents the smallest values. It was found that the torque coefficient decreased by 67%, 77%, 84%, 89%, 94% and 98% for propeller with pitch-to diameter ratios respectively. This could be attributed to the sensitivity of viscous stresses exerted on the propeller blades.

In Figure 4.5 (c) the trend of results of the P/D ratio values were similar for all pitch-to-

diameter ratio and the propeller efficiency profiles had different maximum efficiency with respect to the advance coefficient (J) values. In the Figure 4.5 (c), the efficiency increased by approximately 15% when the pitch-to-diameter ratio increased. It was observed that the maximum efficiency of 73.3% with P/D of 1.6 at advance coefficient of 1.5. This could be attributed to the appropriate assumption that the flow around propeller was fully turbulent. The results showed a small difference of 1% compared to the experimental results of Gawn series (M.Faltinsen, 2006) and Newton-Rader series (Carlton John, 2012). This also strongly agreed with Wageningen-B series marine propeller performance characterization made by M.Bernitsas et al. (M.Bernitsas, Ray, 1981). The same conclusion of increase in efficiency with P/D ratio was also made by Young-Zehr Kehr (Kehr, 1994) while designing the new series propeller for high-speed boats.

4.4 CFD Validation

This section presents the validation of the results obtained in this study. Figure 4.6 compares the results of this study with the experimental results done by Ekinci et al. (Ekinci, 2010). The experiment was done on a conventional DTMB4148-propeller with three blades at the following operating condition, rotational speed of 900rpm and advance coefficient of 0.1 to 0.9. For the DTMB4148 propeller, the available data showed the maximum efficiency of 57.8% took place at J= 0.7 after it declined up to 53.1% at J= 0.9. The numerical results also showed the maximum efficiency of 70% which took place at J = 1.1 after it declines up to 53.9% at J= 1.3. At J= 0.7 the maximum efficiency was 61.9%.

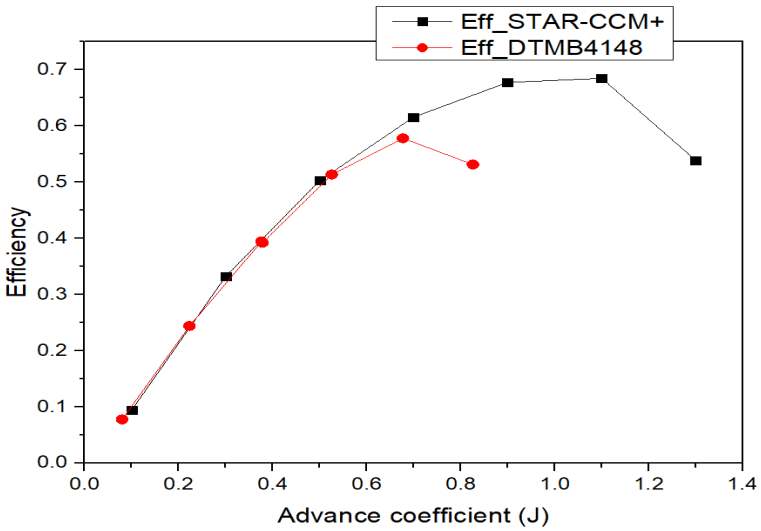

Figure 4.6: Comparison of Experimental and CFD Results For Propeller with Blades

The efficiency had a strong agreement with the experimental results. For the DTMB4148 propeller, the maximum efficiency of 57.8% was obtained at J= 0.7 while 61.9% was obtained at the advance coefficient of 0.7 for simulation results. The numerical results presented an increase of 7.1% as shown in Table 4.1. This could be attributed to the selected fluid domain.

Table 4.1: Comparison of Experimental and CFD Results for Propeller with Three Blades

Z	J	CFD Results	Experimental Data	% Difference
3	0.1	0.09433	0.07761	-2.1
3	0.3	0.33198	0.244028	-3.6
3	0.5	0.50271	0.50055	-4.3
3	0.7	0.61577	0.57811	-7.1
3	0.9	0.67772	0.53167	-2.3
3	1.1	0.68492	-	-
3	1.3	0.53874	-	-

Table 4.2 compares the obtained maximum open water efficiencies to the experimental results of Gawn-series (M.Faltinsen, 2006). The experiment investigated the effect of P/D ratio on propeller performance with three blades. The results obtained from

Table 4.2: Comparison of Experimental and CFD Results for Different P/D

P/D	J	Experimental Data	CFD Results	% Difference
0.6	0.5	0.552	0.565	-2.35
0.8	0.7	0.62	0.652	-5.2
1	0.9	0.65	0.7	-7.7
1.2	1.1	0.651	0.712	-9.4
1.4	1.3	0.706	0.723	-2.3
1.6	1.5	0.74	0.732	1.081

simulation were in good agreement with experimental results. From the Table 4.2, the highest error of 9.4% was obtained at P/D =1.2. The observed error could be attributed to the mesh quality and selected fluid domain.

4.5 Flow Field Analysis on Outboard Propeller

This section presents a flow flied analysis around a marine propeller blade. Velocity and pressure fields around propeller blade were presented following the direction of the fluid flow. The inlet flow was located on the stern to the bow, facing surface (blade front) which is known as pressure side when the boat is advancing forward, the back

of blade is known as the suction side. The velocity and pressure distribution on the propeller blade were also studied.

4.5.1 Velocity Flow Field Around the Blade

Figure 4.7 (a) shows the velocity field of a blade section at advance coefficients (J) of 0.1 and 1.3.

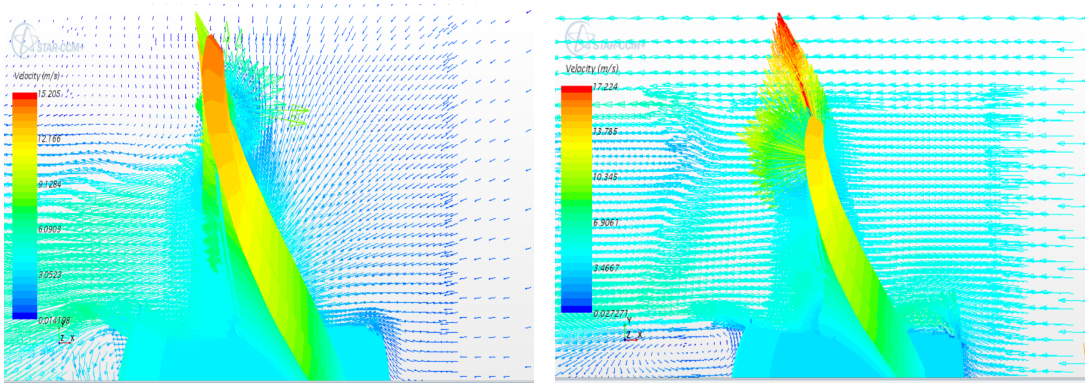

(a) **(b)**

Figure 4.7: Velocity Flow Fields for Advance coefficient (J) of (a) 0.1 and (b) 1.3

For lower advance coefficient (J) of 0.1 shown in Figure 4.7 (a), the water was moving toward the propeller then it was accelerated by the propeller backward as seen near the tip edge of blade. On suction side, velocity fields was symmetric while on pressure side was disturbed.

Figure 4.7(b) shows the velocity field at an advance coefficient of 1.3, high velocity was concentrated at the tip of blade because of the blade rotation. It was also observed that the velocity fields increased by 3.4 m/s from the blade root to the blade tip. The maximum velocity of 17.224 m/s was obtained at the tip at all advance coefficient condition. This was attributed to high loading near the propeller and momentum conservation. This agreed with the findings of Husaini et al. (Husaini et al., 2004) and Wan et al. (Wan, 2014) in propeller design, modeling simulation for an electrical outboard.

4.5.2 Pressure Flow Field Around Blade Section

According to the principle of momentum conservation, when the velocity is high, the pressure drops and vice versa (Johnson, 2011b) . As result, in Figure 4.8 the pressure fields surrounding the blade were created between the pressure and suction sides of the blade at advance coefficient (J) of 0.1 and 1.3, respectively.

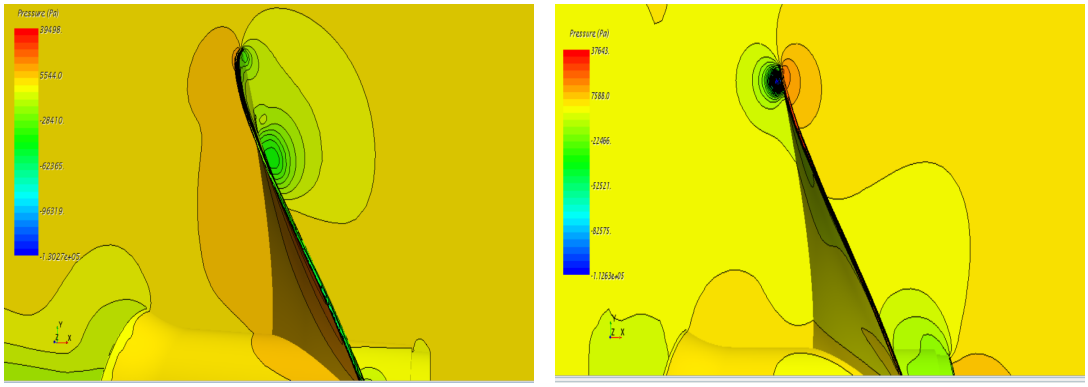

(a) **(b)**

Figure 4.8: Pressure Flow Fields for Advance coefficient (J) of (a) 0.1 and (b) 1.3

In Figure 4.8 (a) (J=0.1), the maximum pressure of 5544.0 Pa was obtained at the tip of the blade of the suction side. The minimum pressure of -62365 Pa was observed at the leading edge of the pressure side of the blade. This could be attributed to the small cross-section that is normal to the flow. This has a good agreement with the findings of Husaini et al. (Husaini et al., 2004) that the pressure increased from root to the tip edge. Shown in Figure 4.8(b) (J=1.3), the maximum pressure of 7588 Pa was found at the tip of the blade of the pressure side. The minimum pressure of -82575 Pa was observed at the tip edge of the suction side. This could be attributed to high loading of the blade near the hub. This agrees with the findings of Martin et al. (Martínez-Calle, Julián González-Pérez & Balbona-Calvo, 2016) while analyzing an open water numerical model for a marine propeller using RANS simulation. The other views are shown in the Appendix B and C.

CHAPTER FIVE
CONCLUSIONS AND RECOMMENDATIONS

5.1 Conclusions

In this study, an outboard marine propeller performance was modeled using computational fluid dynamics method. The effects of number of blade, pitch-to-diameter ratio and rotational speed on an open water propeller performance were investigated. The accuracy of numerical method used in simulation was also evaluated through a comparison of effeciency at different P/D ratios and blade numbers and rotational speed against historical experimental investigations. Based on the outcome of this research, the following conclusions were made:

(a) The decrease in number of the blades increased the propeller efficiency by almost 6%. The maximum efficiency of 70.8% was obtained for a propeller with three blades. It was concluded that a propeller with three blade is suitable as the outboard propulsion system of high-speed boat.

(b) The increase in P/D ratio has an effect on the propeller performance. It increased the propeller efficiency by approximately 15%. The maximum efficiency of 73.3% was obtained for a propeller blade with P/D of 1.6 at the advance coefficient (J) of 1.5. It was concluded that a pitch-to-diameter ratio of 1.6 is suitable in the design of propeller for small high-speed boat running on an outboard engine.

(c) The increase in rotational speeds reduced the propeller thrust coefficient by 57%. The maximum thrust coefficient of 84.8% was obtained for propeller with 900rpm. It was concluded that a propeller with 900rpm is efficient for an outboard propulsion system of high-speed boat.

(d) The maximum velocity and pressure magnitude of 17.224 m/s and 7588 Pa were obtained on the tip edge of propeller blades. At this point flow starts to move in the reverse direction at lower advance coefficient hence different layers region are formed. The layer changed from the pressure to suction side as the propeller loads (advance coefficient) increased. This implies that there is reduction in velocity at the suction side of a propeller blade than the pressure side. It was concluded that the momentum was conserved.

5.2 Recommendations

From this study, the following recommendations were outlined for further study:

(a) For simplicity of the simulation, the propeller performance was done in still water. It is therefore recommended that further work should be done to investigate the propeller performance in moving water.

(b) For high-speed boats, the rotational speed was studied to investigate its impacts on open water characteristics. For further work the parameter affecting the propeller blade cavitation should be investigated to reduce the propeller blade cavitation in outboard propulsion system of high-speed boats.

(c) The effect of the number of blades and pitch to diameter ratio were only studied. It is therefore recommended that for further work, a study should be carried out on the effects of propeller blade specifications such as rake angle, skew angle, blade thickness and blade area ratio in predicting the marine propeller performance.

References

A. Baquero and A.Haimov. (1999). Marine propeller performance: Computational prediction and experimental validation. *Transactions on Modelling and Simulation*, *21*. Retrieved from WITPress,www.witpress.com,ISSN1743-355X

A. Giordani, F. Salvatore, P. E. (1999). Free wake analysis of a marine propeller in uniform flow. *Transactions on Modelling and Simulation*, *24*, 11–21. Retrieved from www.witpress.com

A.H.Techet. (2004). Propeller Notes. *Hydrodynamics for Ocean Engineers*, 1–20.

Am, S. B., M, Y. S., & Fl, S. J. (2005). Advanced Blade Sections for High Speed Propellers. *Inter J Nav Archit Oc Engng*(M), 1–12.

Asimakopoulos, O. A. A. (2016). *Effects of Propeller Geometry on Cavitation* (Doctoral dissertation, Unpublished PhD thesis, Strathclyde: University of Strathclyde 4th). doi: 10.13140/RG.2.1.2863.8325

Assessment and Standards Division Office of Transportation and Air Quality (ASDOTAQ). (2008). Control of Emissions from Marine SI and Small SI Engines, Vessels, and Equipment. *United States Environmental Protection Agency*, 110–139.

Ayris, O. (2016). Effects of Propeller Geometry on Cavitation. *Researchgate*(May). doi: 10.13140/RG.2.1.2863.8325

Barry, C. (2005). Propeller Selection For Boats and Small Ships. *Engines, Mar.*, 1–32.

Bartee, D. L. B., & J., R. (1997). Design of Propulsion Systems for High-Speed Craft. *Marine Technology*, *34*(4), 276–292.

Basumatary Jahnabi, Wood, T. (2017). Cavitation erosion-corrosion in marine propeller materials. *National Centre Of Advanced Tribology (nCATS*(June).

Belhenniche, S. E., Aounallah, M., Omar, I., & Çelik, F. (2016). Effect of Geometric Configurations on Hydrodynamic Performance Assessment of a Marine Propeller. *Brodogradnja*, *67*(4), 31–48. Retrieved from http://hrcak.srce.hr/index.php?show=clanak{&}id{_}clanak{_}jezik=243422{&}lang=en doi: 10.21278/brod67403

Benini, E. (2004). Significance of blade element theory in performance prediction of marine propellers. *Ocean Eng.*, *31*(8-9), 957–974.

Bertetta, D., Brizzolara, S., Canepa, E., Gaggero, S., & Viviani, M. (2012). EFD and CFD Characterization of a CLT Propeller. *International Journal of Rotating Machinery*, *2012*(Article ID 348939), 22. doi: 10.1155/2012/348939

Boucetta, D., & Imine, O. (2016). Numerical Simulation of the Flow around Marine

Propeller Series. *Journal of Physical Science and Application*, *6*(3), 55–61. doi: 10.17265/2159-5348/2016.03.008

Brander, P. (2015). Calculation Results for the 22nd ITTC Propulsor Committee Workshop on Propeller RANS / PANEL Methods : Steady Panel Method Analysis of DTMB 4119 propeller. *Australian Maritime Engineering CRC Ltd*(January).

Bruce, A. L., Ted, R. M., & Maxim, D. L. (2006). Recent Research on Recreational Boating Accidents and the Contribution of Boating Under the Influence. *Pacific Institute for Research & Evaluation*.

Burger, C., John E. Burkhalter, Roy J. Hartfield, Robert S. Gross, & Ronald M. Barrett. (2007). Propeller performance analysis and multidisciplinary optimization using a genetic algorithm. *Auburn University, Alabama*, *Aerospace*(Ph.D. Diss.).

Burrill, L. C. (1944). Calculation of marine propeller performance characteristics. *Transactions of NECIES*, *60:*, 269–294.

Califano, A., & Steen, S. (2011). Numerical simulations of a fully submerged propeller subject to ventilation. *Ocean Engineering*, *38*(14-15), 1582–1599. Retrieved from `http://dx.doi.org/10.1016/j.oceaneng.2011.07.010` doi: 10.1016/j.oceaneng.2011.07.010

Carley, Reg, & Gray, B. (2000). *Boat Handling* (Tech. Rep.).

Carlton John. (2012). Marine Propellers and Propulsion. *Oxford: Butterworth-Heinemann*, 1–142.

Casciani-Wood, J. (2014). Propulsor, Azimuth Propeller, Blade Back, Blade Axis, Blade Centre Line, Blade Centre Face, Blade Number, Blade. *Ocean Engineering*.

CD-Adapco. (2016). User Guide STAR CCM+ v9.06.

Chau, S.-w., Kouh, J.-s., Wong, T.-h., & Chen, Y.-j. (2005). Investigation of Hydrodynamic Performance of High-Speed Craft Rudders via Turbulent Flow Computations. *J. Mar. Sci. Technol.*, *13*(1), 61–72.

Chittaranjan Kumar Reddy, N. R. (2015). Design and Simulation of a Marine Propeller. *Indian J. Mar. Sci.*, *5*(1), 111–128.

Choong, W. H., Yeo, K., Tamiri, F., Tze, K., & Teo, K. (2013). Outboard Marine Propeller Performance Analysis Through CFD Modelling. *UKSim 15th International Conference on Computer Modelling and Simulation Outboard*, 310–313. doi: 10.1109/UKSim.2013.107

Coast, C., Auxiliary, G., & Manual, R. C. (n.d.). Boat Handling. *Ocean Engineering*.

Courtesy of Outboard Marine Corporation. (2001). Operating Outboard Engines. *ABF621-Enginering Knowledge*, 2–7.

Department of the Environment and Water. (2007). Comparative Assessment of the Environmental Performance of Small Engines Marine Outboards and Personal Watercraft. *Environmental Science and Technology*(February).

Dubbioso, G., Muscari, R., & Di Mascio, A. (2014). Analysis of a marine propeller operating in oblique flow. Part 2: Very high incidence angles. *Computers and Fluids*, *92*, 56–81. Retrieved from http://dx.doi.org/10.1016/j.compfluid.2013.01.017 doi: 10.1016/j.compfluid.2013.11.032

Eckhardt, L. C. (1955). Propeller Design Method. *Society of Naval Architecs and Marine Engineers*.

Egerton, J. O., Rasul, M. G., & Brown, R. J. (2007). Outboard Engine Emissions : Modelling and Simulation of Underwater Propeller Velocity Profile using the CFD Code FLUENT. (December), 777–781.

Ekinci, S. (2010). A Practical Noise Prediction Method for Cavitating Marine Propellers. *Brodo Gradnja*, *61*, 359–366.

Erik, D., And, A. H., & Henthorn, B. (2004). *Ethanol as Fuel for Recreational Boats: Final Report* (Tech. Rep. No. March). Thayer School of Engineering at Dartmouth College.

E.Slater, D. R., & John. (1988). *The geometry of Marine Propellers* (Tech. Rep.). Canada: Defence Research Establishment Atlantic.

Favacho, B., Vaz, J., Mesquita, A., Lopes, F., Moreira, A., Soeiro, N., & da Rocha, O. (2016). Contribution to the marine propeller hydrodynamic design for small boats in the amazon region | Contribuição ao projeto hidrodinâmico de propulsores marítimos voltados as pequenas embarcações da região amazônica. *Acta Amazonica*, *46*(1). doi: 10.1590/1809-4392201501723

Felli, M., Guj, G., & Camussi, R. (2008). Effect of the number of blades on propeller wake evolution. *Experiments in Fluids*, *44*(3), 409–418. doi: 10.1007/s00348-007-0385-0

G.A.Butcher. (1985). The effect of Outboard Engine usage and exhaust emissions on the Aquatic Environment.a Review. *Environmental Science and Technology*.

Gaggero, S., Tani, G., Villa, D., Viviani, M., Ausonio, P., Travi, P., ... Serra, F. (2017). Efficient and multi-objective cavitating propeller optimization : An application to a high-speed craft. *Physics Procedia*, *64*, 31–57. Retrieved from http://dx.doi.org/10.1016/j.apor.2017.01.018 doi: 10.1016/j.apor.2017.01.018

Ghasseni, H., & Ghadimi, P. (2011). Numerical analysis of the high skew propeller of an underwater vehicle. *Journal of Marine Science and Application*, *10*(3), 289–299. doi: 10.1007/s11804-011-1071-4

Greco, L., Leone, S., Testa, C., Salvatore, F., & Mauro, S. (2011). Theoretical and Numerical Hydromechanics Analysis of Self-Pitching Propellers. *Second International Symposium on Marine Propulsors*(June).

Griffiths, C. L. (2005). Coastal marine biodiversity in East Africa. *Indian journal of Marine Science*, *34*(March), 35–41.

Gusti, A. P., & Semin. (2016). The Effect of Vessel Speed on Fuel Consumption and Exhaust Gas Emissions. *American Journal of Engineering and Applied Sciences*, *9*(4), 1046–1053. Retrieved from http://thescipub.com/abstract/10.3844/ajeassp.2016.1046.1053 doi: 10.3844/ajeassp.2016.1046.1053

H. Yanagi. (2018). New Medium-term Plan of Outboard Engine markert 2016-2018. *Yamaha Motor Co.Ltd*, 26–34.

Hai-Long, S., Obwogi, E. O., & Yu-Min, S. (2016). Scale effects for rudder bulb and rudder thrust fin on propulsive efficiency based on computational fluid dynamics. *Ocean Engineering*, *117*, 199–209. Retrieved from http://dx.doi.org/10.1016/j.oceaneng.2016.03.046 doi: 10.1016/j.oceaneng.2016.03.046

Hally, D. (2013). Using RANS to Calculate the Flow Past Marine Propellers.

Hanninen, S. (2015). Marine Propeller Model tests Outline. *Aalto University*.

Harte, D., Bose, N., Clifford, R., Roberts, T., & Davidson, G. (2011). An application of paddlewheel propulsion to a high speed craft. *Second International Symposium on Marine Propulsors*(June).

Haynes, J. (2014). Innovative Propulsion Systems for Fast Craft. *Marinelink*, *15*.

Helal, M. M., Ahmed, T. M., & Banawan, A. A. (2018). Numerical prediction of the performance of marine propellers using computational fluid dynamics simulation with transition-sensitive turbulence model. *Journal of Engineering for the Maritime Environment*. doi: 10.1177/1475090218763199

Hong, F. W., & Dong, S. T. (2010). Numerical analysis for circulation distribution of propeller blade. *Journal of Hydrodynamics*, *22*(4), 488–493. Retrieved from http://dx.doi.org/10.1016/S1001-6058(09)60080-9 doi: 10.1016/S1001-6058(09)60080-9

Husaini, M., Samad, Z., & Arshad, M. R. (2004). Autonomous Underwater Vehicle Propeller Simulation using Computational Fluid Dynamic. *Marine Technology*.

International, Z. (2006). *Professional and military Boats* (Tech. Rep.).

International Towing Tunnel Commettee (ITTC). (1993). Final Report and Recommendation of the High-Speed Marine Vehicles Committee. *20th International Towing Tank Conference*.

ITTC. (2011). Recommended Procedures and Guidelines of ITTC. *ITTC media*, 1–8.

Jiang, Y., Sun, H., Zou, J., Hu, A., & Yang, J. (2017). Experimental and numerical investigations on hydrodynamic and aerodynamic characteristics of the tunnel of planing trimaran. *Appl. Ocean Res.*, *63*, 1–10.

John, C. (n.d.). Hydrodynamic Characteristics of Propellers. *International Shipbuilding Progress*, 1–16.

John, C. (2012). Marine Propellers and Propulsion. *Oxford: ButterworthHeinemann*, *2*.

Johnson, E. (2011a). Propeller Selection Guide. *Marinelink*.

Johnson, E. (2011b). Propeller Selection Guide. *Marinelink*.

J.Porteiro Lopez Gonzalez, L. M. (2005). LPG : Pollutant emission and performance enhancement for spark-ignition four strokes outboard engines. *Appl. Therm. Eng.*, *25*, 1882–1893.

Kajishima, T., & Taira, K. (2017). Reynolds-Averaged Navier–Stokes Equations. In *Computational fluid dynamics: Incompressible turbulent flows* (pp. 237–268). Springer International Publishing.

Kamarlouei, M., Ghassemi, H., Aslansefat, K., & Nematy, D. (2014). Multi-Objective Evolutionary Optimization Technique Applied to Propeller Design. *Acta Polytechnica Hungarica*, *11*(9), 163–182.

Kawamura, T., Watanabe, T., Takekoshi, Y., Maeda, M., & Yamaguchi, H. (2004). Numerical Simulation of Cavitating Flow around a Propeller. *Journal of the Society of Naval Architects of Japan*, *2004*(195), 211–219. doi: 10.2534/jjasnaoe1968.2004.195_211

Kehr, Y. Z. (1994). On the Development of a New-Series Propeller for High-Speed Crafts. *Ocean Engineering*.

Kerwin, J. (1986). Marine Propellers. *Annual Review of Fluid Mechanics*, *18*(1), 367–403. Retrieved from `http://fluid.annualreviews.org/cgi/doi/10.1146/annurev.fluid.18.1.367` doi: 10.1146/annurev.fluid.18.1.367

Kerwin, J. E. (2013). Hydrofoils and Propellers - MIT course. *Lecture Notes, Department of Ocean Engineering, Massachusettes Institute Technology, USA*(January).

Kerwin, J. E., & B., J. (2001). 13.04 Lecture Notes Hydrofoils and Propellers. *Cambridge, Massachusetts Institute of Technology*(January).

Kiam Beng Yeo and Wai Heng Choong. (2014). Marine Propeller Geometry Characterization. *Journal of Applied Sciences*, *14*.

Kiam Beng Yeo, Rosalam Sabatly, C. M. O., & Hau, W. Y. (2014). Effects of Marine Propeller Performance and Parameters Using CFD Method. *Journal of Applied*

Sciences, *22*.

Kutty, H., & Rajendran, P. (2017). 3D CFD Simulation and Experimental Validation of Small APC Slow Flyer Propeller Blade. *Aerospace*, *4*(1), 10. Retrieved from http://www.mdpi.com/2226-4310/4/1/10 doi: 10.3390/aerospace4010010

Kutty, H. A., & Rajendran, P. (2008). Review on Numerical and Experimental Work of Conventional and Unconventional Propeller Blade Design. *International Review of Aerospace Engineering (I.RE.AS.E)*, *xx*(July). doi: 10.15866/irease.v10i2.11547

Kuzminski, L. N., & Jackivicz, T. P. (1972). *Interaction of Outboard Motors with the Aquatic Environment Causative Factors and Effects* (Tech. Rep. No. 15).

Lewis, Cleve, H.L Nguyen, H.E. Addy, T.H. Bond, C.M. Lee, , & Chun, K. (1987). Performance and Efficiency Evaluation and Heat Release Study of a Direct Injection Stratified charge Rotary Engine. *N a t i o n a l Aeronautic s and Space A d m i n i s t r a t i o n Research Center and, Ohio 44135*, *SAE 870445*. doi: 10.4271/870445

Li Da-Qing, N. B., & Carl-Erik, J. (2006). Influence of turbulence models on the prediction of full-scale propeller open water characteristics with RANS methods. *26th Symposium on Naval Hydrodynamics*.

MAN Diesel & Turbo. (2011). Basic Principles of Ship Propulsion. *MAN Diesel & Turbo, Copenhagen, Denmark,*.

Marco, A. D., Mancini, S., Miranda, S., Scognamiglio, R., & Vitiello, L. (2017). Experimental and numerical hydrodynamic analysis of a stepped planing hull. *Physics Procedia*, *64*, 135–154. Retrieved from http://dx.doi.org/10.1016/j.apor.2017.02.004 doi: 10.1016/j.apor.2017.02.004

Mario Castro-Cedeno. (2015). *Introduction to SolidWorks* (2nd editio ed.).

Martínez-Calle, Julián González-Pérez, J., & Balbona-Calvo. (2016). An open water numerical model for a marine propeller : a comparison with experimental data. In *Fluids engineering summer conference* (pp. 1–7).

Mashud, K. (2002). Propeller Design. *Journal of the American Society for Naval Engineers*, *36*(4), 693–695. Retrieved from http://teacher.buet.ac.bd/mmkarim/ doi: 10.1111/j.1559-3584.1924.tb05511.x

M.Bernitsas, Ray, K. (1981). *KT, KQ and Efficiency Curves for the Wageningen B-Series Propellers* (Tech. Rep.). Michigan 48109: Department of Naval Architecture and Marine Enginnering, Universit of Michigan Ann Arbor.

M.Bhanu Priya , K.Mohan Krishna, P. (2015). Design and Analysis of Propeller

Blades. *International Research Journal of Engineering and Technology (IRJET)*, 7311–7319. doi: 10.15680/IJIRSET.2015.0408259

Menter, F. R. (1994). Two-Equation Eddy-Viscosity Turbulence Models for Engineering Applications. *AIAA journal*, *32*(8), 1598–1605. doi: 10.2514/3.12149

M.Faltinsen, O. (2006). *Hydrodynamics of High-Speed Marine Vehicles*.

Michael R. Motley, Y. L. (2017). A reliability-based design and optimization of self-twisting composite marine propeller. *European Fluids Engineering Summer Meeting*.

Michigan Wheel Engineering. (2000). Propeller Geometry: Terms and Definitions. *World Leaders in Propulsion and Marine Maneuverability Systems*(August), 18. Retrieved from `http://navalex.com/downloads/Michigan{_}Wheel{_}Propeller{_}Geometry.pdf`

Mintu, M. S. A. (2011). *RANS Computation of Propeller Tip Vortex Flow for Steady and Unsteady Cases* (Unpublished Masters thesis, Nwefoundland:, Memorial University of Nwefoundland). Retrieved from `http://research.library.mun.ca/id/eprint/9668`

Mosaad M.,Mosleh M., E.-K. H., & Yehia. (2017). Guidelines for Numerical Flow Simulation around Marine Propeller. *Researchgate*(March).

Nath, S. P. D. R. (2012). A Computational Method for Determination of Open Water Performance of a Marine Propeller. *International Journal of Computer Applications*, *58*(12), 1–5. Retrieved from `http://www.ijcaonline.org/archives/volume58/number12/9331-3636` doi: 10.5120/9331-3636

Newton-Rader. (1961). Performance Data of Propellers for High Speed Craft. *The Royal Institution of Naval Architects*, *103*(2).

Omweri, O. E., Ondieki, A. J., & Hai-long, S. (2017). Performance prediction of Marine propeller using steady and unsteady flow approaches. In *Proceedings of the sustainable research and innovation conference, jkuat main campus, kenya* (pp. 1–8). Nairobi.

Oosterveld, M., & Van Oossanen, P. (1975). Further Computer-Analyzed Data of The Wageningen B-Screw Series. *International Shipbuilding Progress*, *22*(251), 251–262.

Planchard, D. (2017). SolidWorks 2017 Tutorial with Video Instruction. , 36.

Propellers, Y. (2009). *Outboard Marine Propeller Descriptions* (Tech. Rep.).

Rainbow, H. S. (1963). Some notes on outboard motors. *Inter J Nav Archit Oc Engng*, *178*(1).

Rawson, K. J., & Tupper, E. C. (2010). Basic Ship Theory. *Researchgate*, *2*.

Report, F. (1997). The Propulsion Committee Final Report and Recommendations to the 22nd ITTC. *ITTC media*, 1–53.

RINA. (2011). Cavitation of Propellers. *Stone Mar.*.

S. Barnaby, M. (1897). On the Formation of Cavities in Water by Screw Propellers at High-Speeds. *International Congress of Naval Architects and Marine Engineers*, *58*, 393–418. doi: 10.1063/1.3021091

Salvatore, F., Greco, L., & Calcagni, D. (2011). Computational analysis of marine propeller performance and cavitation by using an inviscid-flow BEM model. (June).

Sánchez-caja, A. (2015). DTRC Propeller 4119 Calculations at VTT. *VTT Tech. Res. Cent. Finl.*, *30*.

Savitsky Daniel, & Ward, B. P. (1976). Procedure of Hydrodynamic Evaluation of Planning Hull in smooth and rough water. *Marine Technology*, *13*(4), 381–400.

Sileo, L., Bonfiglioli, A., & Magi, V. (2006). RANSEs Simulation of the Flow past a Marine Propeller under Design and Off-design Conditions. *Department ofEnvironmental Engineering and Physics, University ofBasilicata Viale dell'Ateneo Lucano 10, 85100 Potenza, Italy*(May 2014).

Steen, S. (2014). Experimental Methods in Marine Hydrodynamics. *Marine Technology Centre Trondheim, Norway*(August).

Sterling, F. W. (1920). *Marine Engineers' Handbook*. McGraw-Hill Book Company, Incorporated.

Subhas, S, V F Saji, S. Ramakrishna, H. N. D. (2012). CFD Analysis of a Propeller Flow and Cavitation. *Int. J. Comput. Appl.*, *55*(16), 26–33.

Tani, G., Villa, D., Gaggero, S., Viviani, M., Ausonio, P., Travi, P., ... Serra, F. (2017). Experimental investigation of pressure pulses and radiated noise for two alternative designs of the propeller of a high-speed craft. *Ocean Engineering*, *132*(January), 45–69. Retrieved from `http://dx.doi.org/10.1016/j.oceaneng.2017.01.015` doi: 10.1016/j.oceaneng.2017.01.015

The Maritime Safety Committee. (1994). HSC Code - International Code of Safety for High Speed Craft, 1994. *International Maritime Organization*, *36*(63).

Tian, Y., & Kinnas, S. (2011). Modeling of Leading Edge Vortex and its Effects on Propeller. *Second Int. Symp. Mar. Propulsors*, *2*(June).

Vesting, F. (2015). *Marine Propeller Optimisation - Strategy and Algorithm Development*.

Wai Heng Choong, K. B. Y., & Hau, W. Y. (2014). Wageningen-B Marine Propeller Performance Characterization Through CFD. *Applied sciences 14*, *11*.

Wan, X. (2014). *Propeller Design , Modeling and Performance Simulation for an Elec-*

tric Outboard (Unpublished Master thesis, Hong Kong:). Hong Kong University of Science and Technology.

Wang, X., & Walters, K. (2012). Computational Analysis of Marine-Propeller Performance Using Transition-Sensitive Turbulence Modeling. *Journal of Fluids Engineering*, *134*(7), 071107. doi: 10.1115/1.4005729

Watanabe, T., Kawamura, T., Takeoshi, Y., Maeda, M., & Rhee, S. H. (2003). Simulation of steady and unsteady cavitation on a marine propeller using a RANS CFD code. *Fifth International Symposium On Cavitation, Osaka, Japan, November 1-4*(July 2014), 1–8.

Webster, K. J. (2015). *Using STAR-CCM + to Evaluate Multi-User Collaboration in CFD* (Unpublished PhD thesis, Chalmers:, Brigham Young University). Retrieved from `https://scholarsarchive.byu.edu/etd/6094`

Wu, X. (2010). A Rapid Development Process for Marine Propellers through Design, Simulation and Prototypimg. *Science, Applied*.

Yang, Y., Zhou, T., Sciacchitano, A., Veldhuis, L., & Eitelberg, G. (2016). Propeller and inflow vortex interaction: vortex response and impact on the propeller performance. *CEAS Aeronautical Journal*, *7*(3), 419–428.

Yao, H., & Zhang, H. (2018). Numerical simulation of boundary-layer transition flow of a model propeller and the full-scale propeller for studying scale effects. *Journal of Marine Science and Technology*, *0*(0), 0. Retrieved from `http://link.springer.com/10.1007/s00773-018-0528-4` doi: 10.1007/s00773-018-0528-4

Yousefi, R., Shafaghat, R., & Shakeri, M. (2013). Hydrodynamic analysis techniques for high-speed planing hulls. *Elsevier*, *42*, 105–113.

Yu, H., Zheng, Y. G., & Yao, Z. M. (2006). The cavitation erosion and erosion-corrosion behavior of carbon steel in simulating solutions of three rivers of China. *Researchgate*, *110016*(9), 705–714. doi: 10.1002/maco.200503958

Zainol, I., & Yaakob, O. (2016). Use of diesel engine and surface-piercing propeller to achieve fuel savings for inshore fishing boats. *Journal of Marine Science and Application*, *15*(2), 214–221. doi: 10.1007/s11804-016-1336-z

Zhao, F., Yang, W., Wan, W., & Kiang, S. (2015). An Overall Ship Propulsion Model for Fuel Efficiency Study. *Energy Procedia*, *75*(65), 813–818. Retrieved from `http://dx.doi.org/10.1016/j.egypro.2015.07.139` doi: 10.1016/j.egypro.2015.07.139

Zhao Yaning. (2015). *Investigation in Scale Effects on Propellers with Different Magnitude of Skew by CFD Methods* (Unpublished doctoral dissertation). Aalwsund

University College.

Zhu, Z.-f., & Fang, S.-l. (2012). Numerical Investigation of Cavitation Performance of Ship Propeller. *J. Hydrodyn.*, *24*(3), 347–353.

APPENDICES

Appendix A: Open Water Propeller Performance Characteristics

The forces and moments produced by the propeller are expressed based on non-dimensional characteristics. These non-dimensional terms that captures the general performance characteristics are established using dimensional analysis (Rawson & Tupper, 2010; Chittaranjan Kumar Reddy, 2015). Thrust (T) and Torque (Q) can be represented by the following functions depending upon the physical quantities involved;

$$T = f_1(\rho, D, V_a, N, \mu, p_o - e) \tag{A.1}$$

Therefore, the thrust (T) can be assumed to be proportional to these values;

$$T = k\rho^a D^b V_a^c N^d \mu^e (p_o - e)^f \tag{A.2}$$

where k is proportional coefficient, and a, b, c, d, e, f are the unknown indices. Since the above equation must be dimensionally consistent, the parameters involved can be replaced by equivalent dimensional terms as shown in Equation A.3

$$\frac{ML}{T^2} = k(\frac{M}{L^3})^a L^b (\frac{L}{T})^c (\frac{1}{T})^d (\frac{M}{LT})^e (\frac{M}{LT^2})^f \tag{A.3}$$

From the equation A.3;

$$\begin{cases} \text{For M: } 1=a+e+f \\ \text{For L: } 1= -3a+b+c-e-f \\ \text{For T: } -2= -c-d-e-2f \end{cases}$$

Hence,

$$\begin{cases} a=1-e-f \\ b=4-c-2e-f \\ d=2-c-e-2f \end{cases}$$

The equation A.2 becomes;

$$T = k\rho^{1-e-f} D^{4-c-2e-f} V_a^c N^{2-c-e-2f} \mu^e (p_o - e)^f \tag{A.4}$$

From which;

$$T = \rho N^2 D^4 (\frac{V_a}{ND})^c (\frac{\mu}{\rho N D^2})^e (\frac{p_o - e}{\rho N^2 D})^f \tag{A.5}$$

These non-dimensional groups are known by the following;
Thrust coefficient,

$$K_T = \frac{T}{\rho N^2 D^4} \tag{A.6}$$

Advance coefficient,

$$J = \frac{V_a}{ND} \tag{A.7}$$

Reynolds number,

$$R_n = \frac{\rho N D^2}{\mu} \tag{A.8}$$

Cavitation number,

$$\sigma_o = \frac{p_o - e}{\frac{1}{2}\rho N^2 D^2} \tag{A.9}$$

when a marine propeller is working sufficiently and submerged deeply enough, the open water characteristics depend upon advance coefficient (J), Reynolds number (Re), and cavitation number (σ). The derivation for propeller torque coefficient (K_Q) is an analogous problem to that of the thrust coefficient just discussed above. The same dependencies in this case can be considered and hence the torque (Q) of the propeller can be considered by writing it as a function of the following terms;

$$Q = f_2(\rho, D, V_a, N, \mu, p_o - e). \tag{A.10}$$

This can be written as;

$$Q = k\rho^a D^b V_a^c N^d \mu^e (p_o - e)^f \tag{A.11}$$

And hence by equating indices the torque coefficient was reduced to;

$$Q = \rho N^2 D^5 (\frac{V_a}{ND})^c (\frac{\mu}{\rho N D^2})^e (\frac{p_o - e}{\rho N^2 D^2})^f \tag{A.12}$$

Torque coefficient,

$$K_Q = \frac{Q}{\rho N^2 D^5} \tag{A.13}$$

The open water efficiency of the propeller is the ratio of useful power produced by the propeller, the thrust horsepower (THP), to the input shaft power, the delivered horsepower (DHP):

$$\eta_o = \frac{THP}{DHP} = \frac{TV_a}{2\pi NQ} = \frac{K_T \rho N^2 D^4 V_a}{2\pi N K_Q \rho N^2 D^5} = \frac{K_T}{K_Q} . \frac{V_a}{2\pi ND} = \frac{K_T}{K_Q} . \frac{J}{2\pi} \tag{A.14}$$

where,
D is the propeller diameter, N is the rotational speed, V_a is the speed advance, ρ is the density of the fluid, μ is the dynamic viscosity of the fluid and g is the gravity.

Appendix B: Mesh Models in STAR-CCM+

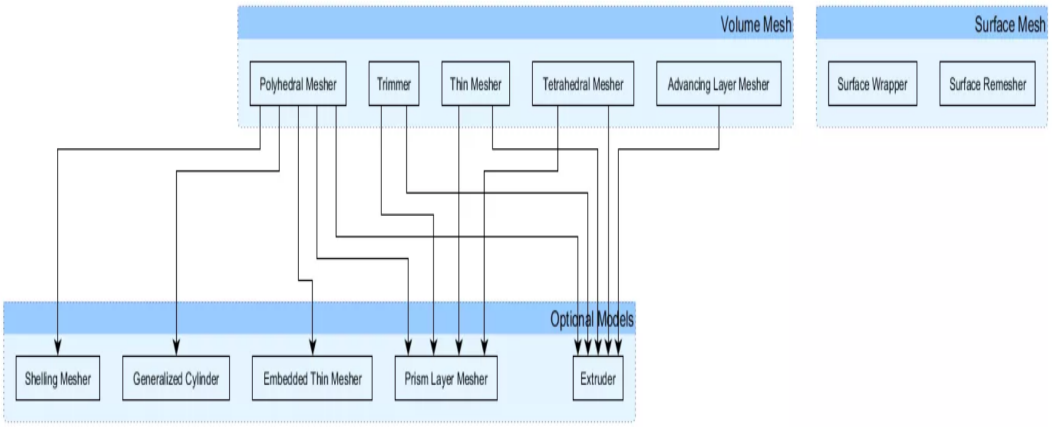

Appendix C: Velocity Vector Field for Different Advance Coefficients

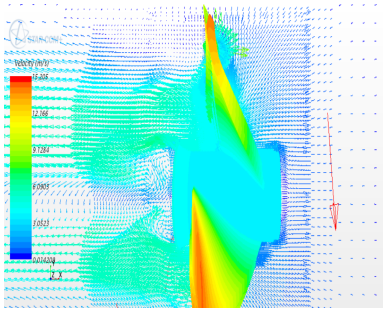

(a) J=0.1

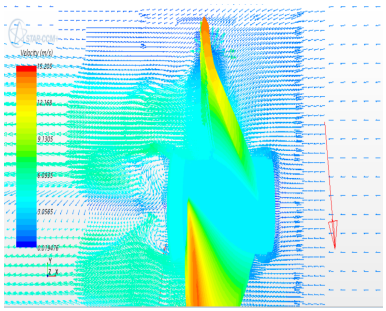

(b) J=0.3

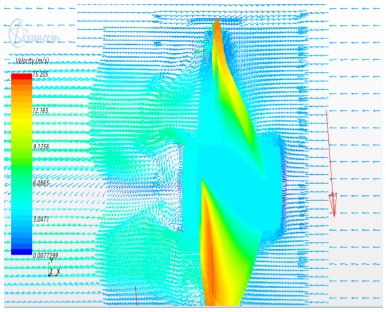

(c) J=0.5

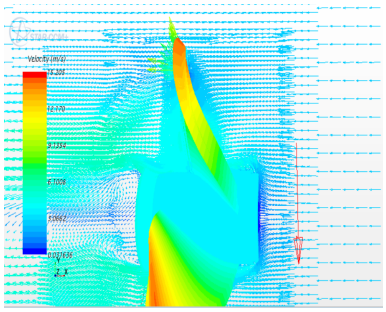

(d) J= 0.7

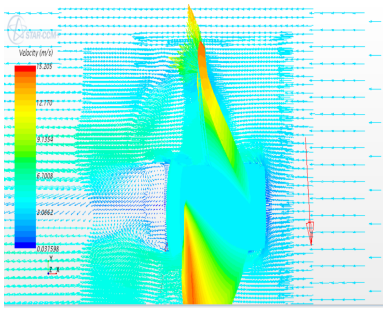

(e) J=0.9

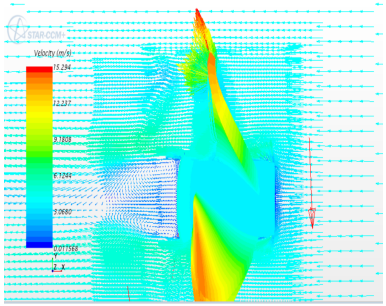

(f) J=1.1

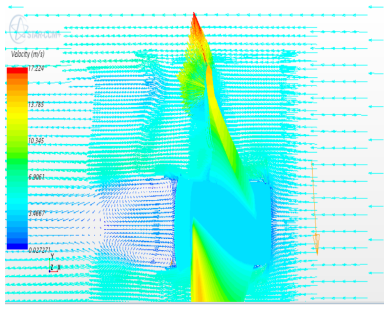

(g) J=1.3

Appendix D: Pressure Flow Field for Different Advance Coefficients

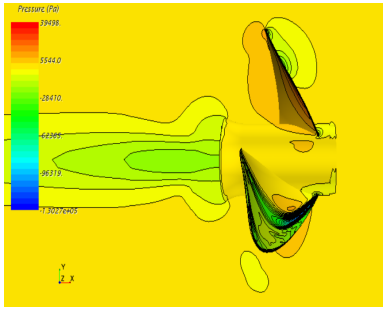

(h) J=0.1

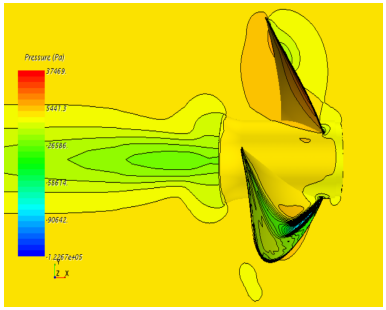

(i) J=0.3

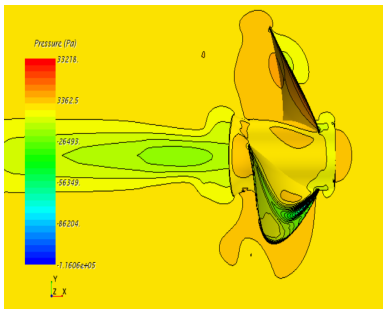

(j) J=0.5

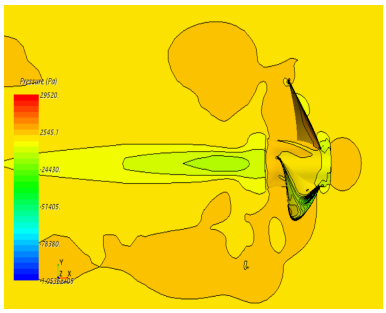

(k) J= 0.7

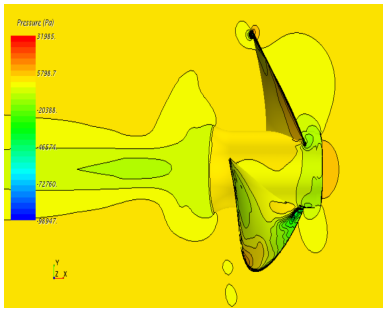

(l) J=0.9

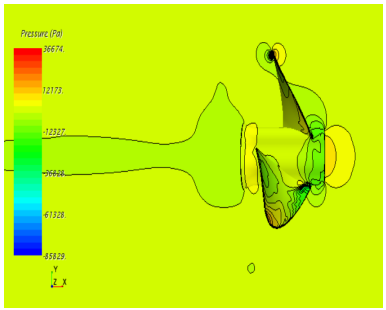

(m) J=1.1

(n) J=1.3